Neurocomputing 556 (2023) 126626

Contents lists available at ScienceDirect

Neurocomputing

journal homepage: www.elsevier.com/locate/neucom

A comprehensive survey on segmentation techniques for retinal vessel segmentation

Jair Cervantes [a,*], Jared Cervantes [a], Farid García-Lamont [a], Arturo Yee-Rendon [b], Josué Espejel Cabrera [a], Laura Domínguez Jalili [a]

[a] UAEMEX (Autonomous University of Mexico State), Texcoco, 56259, Mexico
[b] Facultad de Informática Culiacán, Universidad Autonoma de Sinaloa, Culiacan, Sinaloa, 80013, Mexico

ARTICLE INFO

Keywords:
Vessel segmentation
Preprocessing techniques
Segmentation techniques

ABSTRACT

In recent years, enormous research has been carried out on the segmentation of blood vessels. Segmentation of blood vessels in retinal images is crucial for diagnosing, treating, evaluating clinical results, and early detection of eye disorders. A successful segmentation accurately reflects the blood vessels' structure and helps obtain patterns that can be used to identify retinal disorders and diseases. Most recent research on vessel segmentation employs multiple processes to determine the appropriate segmentation. Finding the best techniques for segmentation is a complex process. In certain circumstances, it requires a thorough understanding of every step that can only be acquired through years of training. Comprehension and expertise in segmentation procedures are essential for accurate segmentation. This paper briefly introduces the segmentation of blood vessels in retinal images, describes many preprocessing and segmentation techniques, and summarizes challenges and trends. Furthermore, the limitations of the current systems will be identified.

1. Introduction

The current development of approaches based on artificial intelligence and digital image processing has been made possible by the growth in the processing power of computers and memory capacity. Many researchers have been interested in developing vision and image processing systems to address challenging issues in real-life scenarios.

Vision systems are widely used in many applications in real life. Vision techniques have been implemented to solve problems in many areas of medicine [1–5]. The processing and analysis of data used in decision-making are aided and facilitated by vision systems. Artificial vision plays a crucial role in medical imaging and healthcare applications. It involves using advanced algorithms to interpret medical images, enabling healthcare professionals to make more accurate diagnoses and provide better patient care. Thus, computer vision algorithms are used in medical image analysis to detect and diagnose specific diseases or conditions.

In neurology, there are computer-aided diagnosis (CAD) systems to help doctors to make rapid diagnoses by classifying normal/abnormal Magnetic Resonance (MR) brain images [6], there are also images acquired from invasive methods like surgeries, craniotomy, and in some cases after the resection of brain tissue for tumor treatments, the images are used not only to segment brain vessels [7] but also to classify tumors and parts of the brain [8], cerebral small vessel disease (SVD) [9–11].

The Oncology area encompasses diverse body organ studies; vessel segmentation can help doctors identify tumor-associated blood vessels more accurately and obtain early diagnosis to select an appropriate treatment. Lung cancer is one of the most common diseases suffered by the people. The vessel segmentation can help in treatment finding the tumor vessels [12,13]. For liver cancer, computer vision can help to obtain the complex of the structure [14–16] and obtain the vessels to irrigate the tumor.

In recent years COVID-19 caught the researcher's attention [17–19]. One of the sequelae of the disease is fibrosis, which can be abroach using the vessel segmentation of the lung arteries. Another kind of fibrosis we can find from human illnesses that medics can improve with vessel segmentation is idiopathic pulmonary fibrosis (IPF) [20,21]

The medical surgery process can be improved using vessel segmentation on medical images, obtaining more accurate diagnoses and more efficient steps in surgical planning using computed tomography (CT) images. From those images, the doctors obtain the vessel's structure, and they can observe anomalies to plan the liver surgery [22]. The vessel segmentation can guide medics with aortic ruptures [23] to plan the surgery.

* Corresponding author.
E-mail addresses: jcervantesc@uaemex.mx (J. Cervantes), jcervantesc002@alumno.uaemex.mx (J. Cervantes), fgarcial@uaemex.mx (F. García-Lamont), arturo.yee@uas.edu.mx (A. Yee-Rendon), jespejelc331@alumno.uaemex.mx (J.E. Cabrera), lydominguezj@uaemex.mx (L.D. Jalili).

https://doi.org/10.1016/j.neucom.2023.126626
Received 8 May 2023; Accepted 24 July 2023
Available online 4 August 2023
0925-2312/© 2023 Elsevier B.V. All rights reserved.

For vascular diseases, vessel segmentation of heart vessels [24,25] can guide the coronary artery disease diagnosis, irregular heartbeats (arrhythmias), or congenital heart defects [26]. For atherosclerosis, vessel segmentation can help to find evidence of vascular disease caused by fat deposits [27,28].

The human vision is a complex process and is an important sense that has to care for; because of the importance of the vision for humans, medics and researchers develop computer-aided diagnosis (CAD) systems for fast diagnosis. Human vision can be affected by many eye-related diseases, such as hypertension, diabetic retinopathy, and arteriosclerosis [29]. The retinal vessel segmentation obtains the shape of the retinal blood vessel, its thickness, and its curvature may indicate some of the mentioned diseases. It is one of the reasons why vessels segmentation is an important task [30,31].

One of the most crucial techniques for identifying diabetic retinopathy, macular degeneration, and early glaucoma diagnosis is blood vessel structure. For the analysis of diseases, the blood vessel structure offers essential information from the shape, orientation, width, curvature, branching patterns, and abnormal region volumes.

Retinal vessel segmentation is commonly performed manually by specialists. This procedure is arduous and complex and requires many years of specialist training. However, manual segmentation consumes too much time and energy. It is susceptible to human error, and noise or light issues that occur when taking the image. All this makes the manual segmentation method unsuitable for large-scale detection. That is why the development of automatic segmentation methods is essential.

The segmentation allows us to obtain the structure of the veins, thickness, proportion, lesions, and other patterns, provide important information about a possible disease and help the specialist to decide on the treatment to be carried out.

Most current research on Vessel segmentation uses several steps to segment accurately. Segmenting the retinal image is difficult because the blood vessels form intricate structures and varied thicknesses. Due to this, the segmentation technique must be chosen appropriately. The quality of the segmentation obtained mainly defines acceptable detection performance.

This paper compares several techniques for the automatic segmentation of blood vessels. It provides essential information on the different algorithms, advantages, disadvantages, and results of the algorithms employed for vessel segmentation.

Furthermore, different algorithms are compared with the most common performance metrics and databases in the state of the art. The results obtained in this article allow a review of the different techniques in the state of the art, analysis, categorize, and provide a source with the necessary information to choose a suitable segmentation technique for vessel segmentation.

The rest of this paper is divided as follows: Section 2 describes retinal images and retinal vessels. Section 3 summarizes the principal databases used in vessel segmentation. Section 4 describes the performance metrics commonly used to evaluate the performance of vessel segmentation. Section 5 Describe the main preprocessing techniques used. Section 6 The principal methods for vessel segmentation are discussed. In addition, their characteristics, advantages, and disadvantages are described. Section 7 shows trends and challenges of vessel segmentation. Finally, Section 8 closes the paper with the conclusions.

2. Retinal images and retinal vessels

Retinal pictures can be taken with a specialized camera with a low-power microscope. The fundus camera can reveal details about the structure of the retina. Images of the retina give a magnified picture of the retina, macula, optic disc, fovea, and blood vessels. Fig. 1 shows the morphology of a retinal image with the principal landmark features.

A fundus camera is defined in terms of its field of view (FOV); 30 to 120 degrees are the FOV ranges commonly used. Higher magnification is available with a lower FOV, but the retina is imaged over a smaller region. A more detailed and in-depth explanation of fundus imaging, Optical coherence tomography imaging, and more is described masterfully in [32,33].

Retinal vessels are the fundamental component of most automated computer-aided methods for detecting retinopathy illnesses. In contrast, manual segmentation of retinal blood vessels is usually a task that is too time-consuming and requires years of specialized training and skill.

A significant amount of current research is focused on accurately extracting the retinal structure; however, it is an open challenge because of many segmentation issues such as illumination during image acquisition, noise, small vessels lost or eliminated due to segmentation, and poor contrast, single vessel segmented as two parallel vessels due to inadequate illumination causing a gap in the segmented vessel, and in comparison parallel vessels segmented as a single large one, and other problems as described in [34–36].

3. Databases

There are several databases used to evaluate the performance of the techniques. However, most of the papers in the state of the art use two databases (Drive and Stare). In this Section, we show the datasets most used to vessel blood segmentation. Table 1 shows a summary of databases commonly used.

DRIVE (Digital Retinal Images for Vessel Extraction). This database includes a total of 40 color fundus photographs, each of which is in JPG format. Seven of the 40 images present exudates, hemorrhages, and pigment epithelium changes. All images were captured with 8 bits per color plane at 768 × 584 pixels, and the 40 images were divided into a test set and a training set, with 20 images [37].

STARE (STructured Analysis of the Retina). The database STARE comprises about 20 images of the retina, of which ten images are classified with pathological features and ten as normal (healthy). The images have 8 bits per color channel and were digitized with a resolution of 650 × 500 pixels [38]. The database contains the hand-labeling of arteries and veins done by two experts.

ARIA (Automatic Retinal Image Analysis), this database allows online analysis of the images, comprising approximately 212 images, where 92 images are classified with age-related macular degeneration, 59 as diabetes, and 61 as a control group. One hundred fifty images are taken for the training set and 40 for the test set. This database was created in 2006; the images are captured in RGB color with 8 bits per color plane and a resolution of 768 × 576 pixels [39].

ImageRet (Image retinopathy), in this database, two subsets of data are included that contain retinal images affected by diabetes. The first is called DIARETDB0. It consists of 130 images, where 20 images are normal and 110 as diabetic retinopathy (DR). In the second subset, DIARETDB1, 89 images are included, where only five are normal, and the other 84 have proliferative diabetic retinopathy. This database was publicly opened in 2006. The images have a resolution of 1500 × 1152 pixels in PNG format [40].

MESSIDOR (Methods to Evaluate Segmentation and Indexing Techniques in Retinal Ophthalmology) is one of the most extensive and complete databases found on the internet. The database contains 1200 images of the retina with several pathologies and images with characteristics of dilated pupils (800 images). Images were obtained with a resolution of 1440 × 960, 2240 × 1488, or 2304 × 1536 pixels and are stored in TIFF format [41].

CHASEDB1. The database contains 28 eye fundus images with a resolution of 1280 × 960. Two sets of ground-truth vessel annotations are available. The first set is commonly used for training and testing. The second set acts as a "human" baseline [42]. It is also available on Kaggle (https://www.kaggle.com/datasets/khoongweihao/chasedb1).

ROC microaneurysm set is one of the most recent databases used in various research works. It contains 100 images of the fundus in color containing microaneurysms, where 50 images are used for the training set and 50 for the test. The images have three different sizes; 768 × 576,

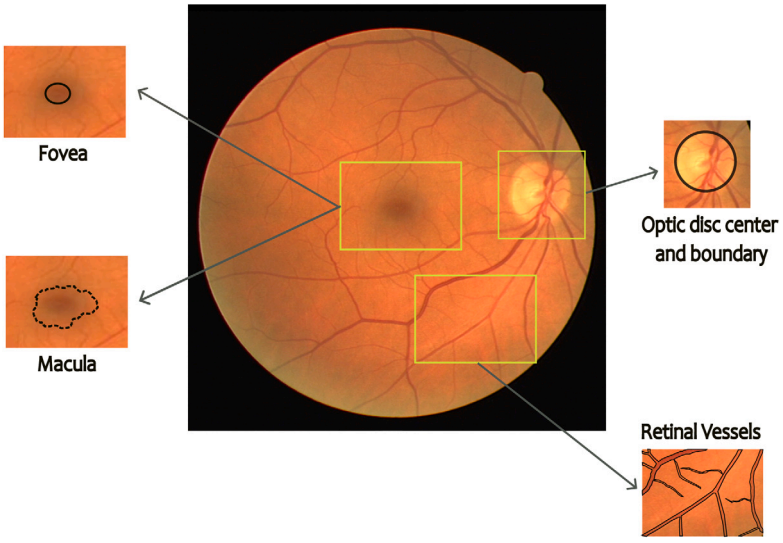

Fig. 1. Important landmark features like the retinal arteries, fovea, macula, and optic disc are shown in the fundus retinal picture.

Table 1
Fundus retinal image databases used to retinal vessel segmentation.

DATABASE	Classes	Size	Resolution
DRIVE	7 diseases 33 normal	40	768 × 584
STARE	10 diseases 10 normal	20	650 × 500
ARIA	151 diseases 61 control group	212	768 × 576
IMAGERET	194 diseases 25 normal	219	1500 × 1152
MESSIDOR	1200 diseases 800 pupil dilation	2000	1440 × 960, 2240 × 1488, 2304 × 1536
CHASEDB1	–	28	1280 × 960
ROC MICROANEURYSM SET	100 diseases	100	768 × 576, 1058 × 1061, 768 × 584
REVIEW	–	16	–
HRF	–	16	3504 × 2368
DR SCREENING INITIATIVE	–	–	2812 × 2442
IOSTAR	–	30	1024 × 1024
RC-SLO	–	40	360 × 320
XCAD	–	40	512 × 512

1058 × 1061, and 1389 × 1383 pixels, and was JPEG compressed in the camera [43].

REVIEW (the Retinal Vessel Image set for Estimation of Widths). The database contains 16 images. The 16 images are grouped into four sets, the high-resolution image set, for its acronym HRIS (8 images). The vascular disease image set, for its acronym VDIS (4 images), the central light reflex image set, for its acronym CLRIS (2 images), and the kick point image set, for its acronym KPIS (2 images) [44].

HIGH-RESOLUTION FUNDUS (HRF) Image Database. The public database contains 16 images of healthy patients, 16 images of patients with diabetic retinopathy, and 16 images of glaucomatous patients. Binary gold standard vessel segmentation images are available for each image. The plane resolution of HRF is 3504 × 2368. Also, the masks determining a field of view (FOV) are provided for particular databases. Experts in retinal image analysis and clinicians from the cooperated ophthalmology clinics generate the gold standard data.

DR SCREENING INITIATIVE. The database has 9653 ungradable retinal images and 11347 gradable images. All images are non-mydriatic, have a 45 degrees FOV and a resolution of 2812 × 2442 pixels. All the images have been graded by human graders, thus confirming their gradability labels.

The IOSTAR vessel segmentation database includes 30 images with a 1024 × 1024 pixels resolution. All the vessels in this database are annotated by a group of experts working in retinal image analysis. Additionally, the database includes annotations for the optic disc and the artery/vein ratio.

Scanning Laser Ophthalmoscopy RC-SLO database from Retina Check contains 40 image patches with a 360 × 320 pixels resolution. Images are acquired with an EasyScan camera (i-Optics Inc., the Netherlands), and all the vessels are annotated by a group of experts working in retinal image analysis.

X-ray angiography coronary artery disease (XCAD) database with coronary angiography images. Each image has a resolution of 512 × 512 pixels with one channel. The training database consists of 1621 mask frames and 1621 coronary angiograms. The testing database contains 126 independent coronary angiograms with vessel segmentation maps annotated by experienced radiologists.

4. Performance metrics

The performance metrics compare the proposed segmented and ground truth images in the blood vessel segmentation process.

There are different metrics to evaluate a segmentation or evaluate pixel classification. The performance also can be expressed in terms of true positives (TP), true negatives (TN), false positives (FP), and false negatives. (FN).

In this context, we will have a segmented image with two crucial areas: the blood vessels, the interest pixels, and the fundus or the surrounding tissue, which are the points of no interest pixels. TP results

if a blood vessel pixel is correctly classified as a vessel and TN if the non-vessel pixel is correctly classified as a non-vessel pixel. In other words, this event happens when background pixels are classified as background.

On the other hand, False positives are the incorrectly identified vessel pixels, and false negatives are the incorrectly identified background pixels.

The performance metrics that we can obtain based on these events are the following:

4.1. Sensitivity (Se)

Sensitivity is also seen as true positive rate (TPR) and can be defined as the proportion of pixels correctly classified as blood vessel pixels [45]. The range of sensitivity has a scale from 0 to 1. Sensitivity can be calculated as follows:

$$Se = \frac{TP}{TP + FN} \tag{1}$$

4.2. Specificity (Sp)

Specificity is also seen as True negative rate (TNR) can be defined as the proportion of pixels correctly classified as non-vessel pixels. The range is between 0 and 1. Specificity can be calculated as:

$$Sp = \frac{TN}{TN + FP} \tag{2}$$

4.3. Accuracy (Acc)

Accuracy is the relation of the sum of TP and TN among the total number of pixels or the sum of TP, TN, FP, and FN. The mathematical expression is as follows:

$$Acc = \frac{TP + TN}{TP + TN + FP + FN} \tag{3}$$

4.4. A false positive rate (FPR)

FPR is the complement of specificity and can be defined as the proportion of pixels wrongly classified as blood vessels. FPR can be calculated using two formulas:

$$FPR = \frac{FP}{TN + FP} \tag{4}$$

$$FPR = 1 - Sp \tag{5}$$

4.5. Area under curve (AUC)

In this concept, the important point is the area. This area is formed under the curve, commonly called the Receiver Operating Characteristic (ROC) curve. The ROC curve plots the graph between sensitivity and the portion of non-vessel pixels wrongly assigned as vessels (FPR). The value of the area under the curve (AUC) should be 1 for a model that classifies the examples perfectly and 0.5 for a model with a purely random guess.

4.6. Matthews correlation coefficient (MCC)

MCC is a tool for measuring a binary classification or a segmentation and measures the differences between the actual and predicted values. The formula used to calculate this coefficient is as follows:

$$Mcc = \frac{(TN * TP) - (FN * FP)}{\sqrt{(TP + FP)(TP + FN)(TN + FP)(TN + FN)}} \tag{6}$$

5. Preprocessing techniques

Image preprocessing is a crucial step in almost all vessel segmentation techniques. Preprocessing operations do not add information to the image. The main purpose of the preprocessing methods is to remove or suppress unwanted distortions and highlight relevant information. These operations are used, taking care not to delete essential information. Some examples of image preprocessing include Color and space color selection, Brightness corrections, Image Filtering, and restoration.

The inappropriate use of image preprocessing may distort the image and change the nature of the raw data. However, intelligent use of image preprocessing can have dramatic positive effects on the quality of segmentation and ultimately lead to better local or global feature detection and image analysis results.

Some researchers use different image preprocessing techniques to improve the segmentation performance. Chaudhuri [46] proposed an algorithm where image enhancement is done before the segmentation of vessels using a 5×5 mean filter which reduces the effect of spurious noise. Marin et al. [47]. In this research, the original image is preprocessed first to reduce improper illumination in the image and remove the vessel central light reflex problem. The Gaussian kernel is used to smooth the noise. In their experiments, the authors use several types of filters of different sizes (mean filter 3×3, Gaussian kernel 9×9, and mean filter 69×69). Ocbagabir et al. [48] improved the blood vessels by using techniques of preprocessing and postprocessing with morphological operations and Adaptive Histogram Equalization. The median filtering technique is used to remove noise.

Moccia et al. [49] In their research, they works with a flow of vessel segmentation, where, from an in-depth analysis, improvement approaches in blood vessels are highlighted. Therefore, it describes the preprocessing of images as a normalization of the data in an image and, likewise, improves the contrast. In this stage, the images are processed through various procedures such as global contrast and data augmentation through geometric transformations and gamma corrections.

Fraz et al. [50] use a combination of certain preprocessing techniques. First, morphological operators are applied, and with the help of an SVM, this technique uses the green channel of the image. Wavelets are used to process the original image and highlight the blood vessels. The familiar line detectors are used to highlight the thinnest blood vessels.

Biradar and Jadhav [51] propose an automated method to identify the optic disc based on two methodologies: a localization methodology and a boundary segmentation methodology. The authors use morphological processing and a Gaussian filter to obtain adequate segmentation, eliminating the image's existing noise.

Before the segmentation process, image preprocessing is used to remove bad lighting effects and different types of noise, besides increasing the contrast between the background and the retinal blood vessels. Preprocessing and postprocessing techniques play an important role in accurate segmentation. In this Section, we describe the preprocessing techniques most used in the state of the art.

5.1. Brightness correction

5.1.1. Gamma correction

Gamma correction adjusts the brightness of an image by applying a nonlinear function to the pixel values in the input image. Gamma correction improves contrast and detail in an image by making dark regions brighter and bright regions darker. The effects in the image cause it to be perceived as more realistic and natural.

The new pixel values $N(k)$ in an image can be obtained by

$$N(k) = O(k)^{\frac{1}{\gamma}} \tag{7}$$

where $N(k)$ represents the kth pixel value in the output image and $O(k)$ represents the kth pixel value in the input image. and γ is the gamma

correction, which determines the degree of correction. A gamma factor greater than one will darken the image, while a gamma factor less than one will lighten it. However, in most real-life applications, the gamma correction ranges between 1.8 and 2.5.

5.1.2. Histogram equalization

Histogram equalization is a non-linear process technique that adjusts the distribution of pixel values in an image, obtaining a smooth histogram in the output image. Histogram equalization can be applied to color or grayscale images. However, in color images, it can affect color balance and saturation.

An image in greyscale in 8 bits has 255 intensity levels, $k = (0, 1, 2, \dots, 255)$ and the probability density in the input image for the intensity x_k is $p_x(x_k)$. The cumulative histogram is given by

$$y(x_k) = \sum_{j=0}^{k} p_x(x_k) \tag{8}$$

where $y(x_k)$ is the sum of all the histograms bins from $k = 0$ to the actual k for the image x The new pixel values $y(k)$ in an image can be obtained by

$$y(k) = \sum_{j=0}^{k} p_x(j) = \frac{1}{N} \sum_{j=0}^{k} n_x(j) \tag{9}$$

where k the population of the kth level is given by n_k and the total number of pixels in the image is N.

5.1.3. Sharpening filters

Sharpening filters are techniques that improve an image's sharpness by highlighting objects' edges and boundaries. Obtaining clear images and crisps because sharpening filters reduce blur caused by camera movement or focus. One of their advantages is that they can highlight the texture and detail in an image by increasing the contrast between adjacent pixels.

To implement sharpening filters, a template convolution operator is necessary, commonly called kernel. The kernel is a matrix that describes the weight of each neighbor in the new pixel. A common sharpening filter is the Laplacian filter. The following two small kernels are frequently used:

$$L_1 = \begin{bmatrix} 0 & 1 & 0 \\ 1 & -4 & 1 \\ 0 & 1 & 0 \end{bmatrix} \qquad L_2 = \begin{bmatrix} 1 & 1 & 1 \\ 1 & -8 & 1 \\ 1 & 1 & 1 \end{bmatrix}$$

The center of the kernel subtracts the average of the neighboring pixels from the center pixel, which amplifies the difference between them.

5.1.4. Contrast limited adaptive histogram equalization (CLAHE)

CLAHE is a variant of Adaptive Histogram Equalization (AHE) that deals with local contrast over-amplification. In other words, it is a handy algorithm for enhancing low contrast in an image. The main job of this algorithm is eliminating noise, taking full advantage of the spectrum of gray levels, and giving greater precision in contrast details by generating sharper edges.

Unlike other algorithms, CLAHE does not operate on the entire image. It is developed in small regions of the image called mosaics. Neighboring tiles are then combined using bilinear interpolation to remove artificial boundaries.

The benefits of CLAHE are most noticeable in color images, where it is commonly applied to the luminance channel, and the results after equalizing only the luminance channel of an HSV image are much better than equalizing all channels of the RGB image. Fig. 2 (c) shows an image using the CLAHE algorithm.

5.2. Image filtering

Image filtering can modify the digital image values of each pixel p by a function of the neighbor's value and the pixel p known as convolution mask or kernel. The size of the kernel determines the extent of the neighborhood considered during convolution, common kernel sizes include 3×3, 5×5, and 7×7.

5.2.1. Mean filter

The mean filter is a linear filter used for image smoothing and noise reduction by replacing the value of each pixel in an image with the average value of its neighboring pixels. The larger the kernel proportionally influences, the stronger the smoothing effect, but it can also cause a loss of image details. The convolution operation using the mean filter can replace each pixel by a weighted average of its neighborhood pixels as follows:

$$v(m, n) = \sum \sum_{(k,l) \in W} a(k, l) y(m - k, n - l) \tag{10}$$

where $y(m, n)$ y $v(m, n)$ are the input and output images respectively, W is the window selected, and $a(k, l)$ are the filters weights.

5.2.2. Median filter

The median filter is commonly seen as smoothers in digital image processing. Among its advantages is its ability to attenuate noise and robustness and preserve sharp high-frequency details (edges). The biggest advantage of the median filter is that it can eliminate the effect of input noise values with very large magnitudes.

$$v(m, n) = median\,[y(m - k, n - l), (k, l) \in W] \tag{11}$$

where W is the window selected.

5.2.3. Gaussian filter

Gaussian filters reduce noise and smooth an image. The values in the Gaussian kernel are determined by the Gaussian function, which gives more weight to the central pixel and gradually reduces the weight as the distance from the central pixel increases, which creates a blurring effect, where sharp transitions and noise in the image are smoothed out.

The formula for the 2D Gaussian function is given by:

$$v(m, n) = \frac{1}{2\pi\sigma^2} e^{-\frac{m^2+n^2}{2\sigma^2}} \tag{12}$$

5.2.4. Gabor filter

Gabor filters is a linear filter used for edge detection. Gabor filters have frequency-selective and orientation-selective properties and have optimal joint resolution in both spatial and frequency domains. The Gabor filter is used for texture discrimination and representation.

5.3. Morphologic operators

5.3.1. Dilation and erotion

Image A may still contain pixels that belong to the background, to remove them without altering the characters, the image is eroded:

$$A_e = A \ominus B = (x', y') \mid (x' + i,' + j) \in P_A, (i, j) \in P_B \tag{13}$$

Where A is the original image, A_e is the eroded image, and $\ominus$ denotes the eroding operator using the mask B.

Now the morphological dilation operation is used to restore possible broken or incomplete characters. This can be done using the following operator:

$$A_d = A \oplus B = (x', y') = (x + i, y + j) \mid (x', y') \in P_A, (i, j) \in P_B \tag{14}$$

Fig. 2. Vessel segmentation: (a) Original retinal fundus image ("Image_01L.jpg" from Chase Database), (b) green channel of the original image, (c) Enhanced image using CLAHE, (d) Manual segmentation ("Image_01L_1stHO.png" from Chase database).

5.3.2. Methods to eliminate noise in binary images

Among the morphological operations, some techniques serve to eliminate noise in images. The following equations allow us to carry out this work.

1. Remove noise (black dots) from white areas.

$$P_0 = P + (b \cdot g \cdot (d + e) + (d \cdot e \cdot (b + g))) \tag{15}$$

2. Remove noise (white dots) from black areas.

$$P_0 = P + (((a + b + d) \cdot (e + g + h)) + ((b + c + e) \cdot (d + f + g))) \tag{16}$$

3. Reconstruct corners of white images.

- Upper right

$$P_0 = \bar{P} \cdot d \cdot f \cdot g \cdot \overline{(a + b + c + e + h)} + P \tag{17}$$

- lower right.

$$P_0 = \bar{P} \cdot a \cdot b \cdot d \cdot \overline{(e + c + f + g + h)} + P \tag{18}$$

- Upper left.

$$P_0 = \bar{P} \cdot e \cdot g \cdot h \cdot \overline{a + b + c + d + f} + P \tag{19}$$

- Lower left.

$$P_0 = \bar{P} \cdot b \cdot c \cdot e \cdot \overline{a + d + f + g + h} + P \tag{20}$$

4. Reconstruct corners of black images

- Upper right

$$P_0 = \bar{P} \cdot (d + f + g) + \overline{a \cdot b \cdot c \cdot e \cdot h \cdot P} \tag{21}$$

- Lower right.

$$P_0 = \bar{P} \cdot (a + b + d) + \overline{c \cdot e \cdot f \cdot g \cdot h \cdot P} \tag{22}$$

- Upper left.

$$P_0 = \bar{P} \cdot (e + g + h) + \overline{a \cdot b \cdot c \cdot d \cdot f \cdot P} \tag{23}$$

- Lower left.

$$P_0 = \bar{P} \cdot (b + c + e) + \overline{a \cdot d \cdot f \cdot g \cdot h \cdot P} \tag{24}$$

5.4. Color transformations

5.4.1. RGB to HSV

Mapping the RGB space to HSV space color, given $\Phi = [r, g, b]$ the color vector in RGB space and $\varphi = [h, s, v]$ the resulting vector when mapping Φ into the HSV space.

$$\Theta = \begin{cases} undefined, & r = g = b \\ \cos^{-1}\left(\frac{(r-g)+(r-b)}{2\sqrt{(r-g)^2+(r-b)(g-b)}}\right), & otherwise \end{cases} \tag{25}$$

$$h = \begin{cases} \theta, & b \le g \\ 2\pi - \theta, & b > g \end{cases} \tag{26}$$

$$s = \begin{cases} 0, & max(r, g, b) = 0 \\ 1 - \frac{min(r,g,b)}{max(r,g,b)}, & otherwise \end{cases} \tag{27}$$

$$v = max(r, g, b) \tag{28}$$

5.4.2. HSV to RGB

Mapping the HSV space into the RGB space, given the color vector in the HSV space $\varphi = [h, s, v]$ and $\Phi = [r, g, b]$ the resulting vector when mapping φ into RGB space: if $h = undefined$ then $r = v$, $g = v$ and $b = v$ otherwise

$$r = \begin{cases} q, & k = 1 \\ p, & 2 \le k \le 3 \\ t, & k = 4 \\ v, & otherwise \end{cases} \tag{29}$$

$$g = \begin{cases} t, & k = 0 \\ v, & 1 \le k \le 2 \\ q, & k = 3 \\ p, & otherwise \end{cases} \tag{30}$$

$$b = \begin{cases} p, & 0 \le k \le 1 \\ t, & k = 2 \\ v, & 3 \le k \le 4 \\ q, & otherwise \end{cases} \tag{31}$$

where:

$$k = \left\lfloor \frac{3}{\pi} h \right\rfloor \tag{32}$$

$$f = \frac{3}{\pi} h - k \tag{33}$$

$$p = v \times (1 - s) \tag{34}$$

$$q = v \times (1 - (s \times f)) \tag{35}$$

$$t = v \times (1 - (s \times (1 - f))) \tag{36}$$

5.4.3. RGB to HSI

Mapping the RGB space into the HSI space, given $\Phi = [r, g, b]$ RGB color and $\varphi = [h, s, i]$ is the resulting vector of mapping Φ into the HSI space:

$$\Theta = \begin{cases} undefined, & r = g = b \\ \cos^{-1}\left(\frac{(r-g)+(r-b)}{2\sqrt{(r-g)^2+(r-b)(g-b)}}\right), & otherwise \end{cases} \tag{37}$$

$$h = \begin{cases} \theta, & b \le g \\ 2\pi - \theta, & b > g \end{cases} \tag{38}$$

$$s = 1 - \frac{min(r, g, b)}{i} \tag{39}$$

$$i = \frac{r + g + b}{3} \tag{40}$$

5.4.4. HSI to RGB

Mapping the HSI space into the RGB space, given the HSI vector color $\varphi = [h, s, i]$ and $\Phi = [r, g, b]$ is the resulting vector of mapping φ into RGB space:

If $h = undefined$ then $r = i$, $g = i$ and $b = i$. If $0 \leq h < \frac{2}{3}\pi$ then

$$b = i(1 - s) \tag{41}$$

$$r = i\left(1 + \frac{s\cos h}{\cos\left(\frac{\pi}{3} - h\right)}\right) \tag{42}$$

$$g = 3i(1 - r - b) \tag{43}$$

If $\frac{2}{3}\pi \leq h < \frac{3}{4}\pi$ then

$$r = i(1 - s) \tag{44}$$

$$g = i\left(1 + \frac{s\cos\left(h - \frac{2}{3}\pi\right)}{\cos(\pi - h)}\right) \tag{45}$$

$$b = 3i(1 - r - g) \tag{46}$$

If $\frac{4}{3}\pi \leq h < 2\pi$ then

$$g = i(1 - s) \tag{47}$$

$$b = i\left(1 + \frac{s\cos(h - \frac{4}{3}\pi)}{\cos(\frac{5}{3}\pi - h)}\right) \tag{48}$$

$$r = 3i(1 - g - b) \tag{49}$$

5.4.5. RGB to L*a*b

To transform RGB space into the L*a*b, given $\Phi = [r, g, b]$ the RGB color vector and $\varphi = [l, a, b]$ is the resulting color vector of mapping Φ into L*a*b space

$$L^* = 116 f(\frac{Y}{Y_{ref}}) - 16 \tag{50}$$

$$a^* = 500\left[f(\frac{X}{X_{ref}}) - f(\frac{Y}{Y_{ref}})\right] \tag{51}$$

$$b^* = 200\left[f(\frac{Y}{Y_{ref}}) - f(\frac{Z}{Z_{ref}})\right] \tag{52}$$

$$\begin{bmatrix} X \\ Y \\ Z \end{bmatrix} = \begin{bmatrix} 0.4124 & 0.3575 & 0.1804 \\ 0.2126 & 0.7151 & 0.0721 \\ 0.0193 & 0.1191 & 0.9502 \end{bmatrix} \begin{bmatrix} r \\ g \\ b \end{bmatrix} \tag{53}$$

where $\delta = \frac{6}{29} y$

$$f(t) = \begin{cases} \sqrt[3]{t}, & t > \delta^3 \\ \frac{t}{3\delta^2} + \frac{4}{29}, & t \leq \delta^3 \end{cases} \tag{54}$$

5.4.6. L*a*b to RGB

The inverse operation is defined by

$$X = X_{ref} h(\frac{L^* + 16}{116} + \frac{a^*}{500}) \tag{55}$$

$$Y = Y_{ref} h(\frac{L^* + 16}{116}) \tag{56}$$

$$Z = Z_{ref} h(\frac{L^* + 16}{116} - \frac{b*}{200}) \tag{57}$$

where

$$h(t) = \begin{cases} t^3, & t > \delta \\ 3\delta^2(t - \frac{4}{29}) & t \leq \delta \end{cases} \tag{58}$$

$$\begin{bmatrix} r \\ g \\ b \end{bmatrix} = \begin{bmatrix} 0.4121 & 0.3575 & 0.1804 \\ 0.2126 & 0.7151 & 0.0721 \\ 0.0193 & 0.1194 & 0.9502 \end{bmatrix}^{-1} \begin{bmatrix} Y \\ X \\ Z \end{bmatrix} \tag{59}$$

The values X_{ref}, Y_{ref} and Z_{ref} are obtained replacing the tristimulus values for white reference.

6. Segmentation techniques

Digital image processing (DIP) focuses on developing algorithms to perform processing on an image. The principal types of images processing are: Visualization [52], Recognition [53–59], Sharpening and restoration [60], Pattern recognition [61–64] and Retrieval [65,66].

One of the most challenging elements of DIP is still image segmentation [67,68]. Segmentation is the building block of many algorithms in computer vision and pattern recognition, whose main goal is to perform sophisticated visual analysis and understanding. The effectiveness of the pattern recognition or vision system is based on image segmentation. Segmentation is crucial for adequate feature extraction [69–71]. Image properties such as brightness, color, depth, pixel intensity, and texture are commonly used by the image segmentation algorithms [72].

Segmentation techniques based on Edge detection, threshold, histogram-thresholding, region growing, clustering, and neural networks are a few vessel segmentation techniques presented in the literature [73]. In this paper, we provide a number of research that use these strategies, but we also present comparable studies that make use of alternative methodologies.

6.1. Methods based on threshold

This subsection shows the most important threshold techniques: Mean-C thresholding, hysteresis thresholding, Global threshold, adaptive threshold, and Otsu thresholding method.

6.1.1. Mean-C thresholding

Most thresholding segmentation techniques are simple but effective tools to separate objects from the background. Mean-C thresholding is proposed in [74], and it is a simple thresholding segmentation technique whose main advantage is that it is applicable in badly illuminated images.

The mean-C thresholding technique calculates a threshold for each pixel in the image based on local statistics. The threshold is calculated using the following steps. A mean image is first generated by convolving the image with a mean filter of window size $N \times N$. The mean filter smooths the background and enhances the image. Next, the mean-filtered image is subtracted from the original image to produce a different image. The image is thresholded with the constant value C which is selected appropriately.

6.1.2. Hysteresis thresholding

Thresholding methods use one threshold to segment; hysteresis thresholding methods use two thresholds T_{low} and T_{high}. Standard thresholding methods convert any intensity below the border to black and above it to white. On the other hand, the Hysteresis thresholding uses various considerations to segment the image, allowing for there to be fewer white segments in the resulting image. This process improves, in many cases, the resulting segmentation.

6.1.3. Global threshold

Intensity thresholding is the most basic idea in segmentation; the technique is an extreme form of gray-level quantization. Global threshold creates a binary image $b(x, y)$ from an image $I(x, y)$ according to a simple criterion.

$$b(x, y) = \begin{cases} 1, & I(x, y) > th \\ 0, & otherwise \end{cases} \tag{60}$$

where th is the threshold. Global threshold is a fast segmentation technique with low computational cost.

6.1.4. Adaptive threshold

The proper threshold level setting for the global threshold approach is a serious factor. These settings are often chosen manually through trial and error. However, many processing tasks are required to select a threshold automatically.

Sonka provides information on an adaptive method for automatic threshold in [75]. First, the threshold is estimated, often by determining the mean grey level across the entire image. Then the threshold is then improved using Algorithm 1.

Algorithm 1 Adaptive threshold algorithm

Input: Image I
Output: Threshold T

1: Compute μ_1, the mean gray level of the whole image
2: $T_{old} = 0$
3: $T_{new} = (\mu_1 + \mu_2)/2$
4: **while** $T_{old} \neq T_{old}$ **do**
5: μ_1 = mean gray level of pixels for which $I(x, y) < T_{new}$
6: μ_2 = mean gray level of pixels for which $I(x, y) \geq T_{new}$
7: $T_{old} = T_{old}$
8: $T_{new} = (\mu_1 + \mu_2)/2$
9: **end while**

The algorithm is iterated recursively until the threshold stops changing. The threshold has then gotten to its best estimation value.

6.1.5. Otsu method

Otsu's method is important because it can work on images with noise and poor lighting. The main advantage is that it is an automatic method whose application does not require human supervision or prior information. Several methods exist to find the threshold based on the average of the gray levels in a binary image. However, Otsu's method is a sophisticated way of obtaining the threshold compared to traditional methods.

This sophistication comes from minimizing the weighted intra-class variance and maximizing the inter-class variance by passing through all possible threshold values. In this Section, the operation of the Otsu algorithm is shown in Algorithm 2.

It should be noted that this method does not require prior information on the image before processing and does not require human supervision to calculate thresholds. where $C_0 \subset \{1, \ldots, k\}$ and $C_1 \subset \{k+1, \ldots, L\}$ define the intensity levels of each set. w_0 and w_1 are computed by $w_0(t) = P_r(C_o) = \sum_{i=1}^{k} P(i) = w(k)$ and $w_1(t) = P_r(C_1) = \sum_{i=k+1}^{L} P(i) = 1 - w(k)$ respectively. The means for C_1 and C_2, are calculated by

$$\mu_0(t) = \sum_{i=1}^{k} i P_r(i \mid C_0) = \sum i \frac{P(i)}{w_0(t)} = \frac{\mu k}{w(k)} \tag{61}$$

$$\mu_1(t) = \sum i P_r(i \mid C_1) = \sum_{i=k+1}^{L} i \frac{P(i)}{w_1(t)} = \frac{\mu_T}{1 - w(k)} \tag{62}$$

Algorithm 2 Otsu algorithm

Input: Image I
Output: Threshold T

1: Compute P_i, the probability of occurrence of the gray level of an image, $P_i = \frac{n_i}{M \times N}$, n_i = number of pixels with level intensity i
2: Compute the accumulative sum $P_i(k) = \sum_{k=0}^{k} p_i$, where k = 0,1,...,L-1
3: **for all** $k = 2, ..., L-1$ **do**
4: Define C_0 and C_1
5: Compute w_0 and w_1
6: Compute μ_0 and μ_1
7: Obtain $max_k(\sigma_w^2)$
end for

The variance is calculated by

$$\sigma_0^2 = \sum_{i=1}^{k} (i - \mu_0)^2 Pi(i \mid C_0) = \sum_{i=1}^{k} \frac{(i - \mu_0)^2 Pi}{w_0} \tag{63}$$

$$\sigma_1^2 = \sum_{i=k+1}^{L} (i - \mu_1)^2 Pi(i \mid C_1) = \sum_{i=1}^{L} \frac{(i - \mu_1)^2 Pi}{w_1} \tag{64}$$

Finally, we get the threshold for which σ_w^2 has the maximum value

$$\sigma_w^2 = w_0 \sigma_0^2 + w_1 \sigma_1^2 \tag{65}$$

Minimizing the intra-class variance is equivalent to maximizing inter-class variance

$$\sigma_b^2 = \sigma^2 - \sigma_w^2(t) \tag{66}$$

$$= w_0(t)(\mu_0 - \mu_T)^2 + w_1(t)(\mu_0 - \mu_T)^2 \tag{67}$$

$$= w_0(t) w_1(t) [\mu_0(t) - \mu_1(t)]^2 \tag{68}$$

Several researchers use the Otsu method to segment vessels' blood images. Thresholding methods are popular due to their robustness, simplicity, and accuracy.

In [76], the authors proposed an unsupervised approach using a combination of the Hessian-based and intensity transformation approaches. The authors used Otsu to segment thick vessels and local thresholds to obtain thin vessels. The authors use some preprocessing techniques to clean and enhance the image. CLAHE is used to improve the contrast in the image, and a PSO algorithm is used to obtain the optimal parameters of CLAHE. Morphological filter and Wiener filter are used to de-noise the image. The authors use an intensity transformation approach to the enhanced image to maximize the vessel details.

In [77] was proposed a new framework using CLAHE, morphological filter, and hessian matrix as preprocessing techniques. The authors segment wide and thin vessels in two steps using Otsu thresholding. The authors argue that the framework performs efficiently against noise and extract thin vessels. The proposed method is robust and computationally efficient.

Jiang et al. [78] combined matched filtering and morphological processing techniques. The proposed framework achieves higher accuracy and better robustness, and the authors argue that it decreases the computing complexity and shortens the execution time. The image is used in greyscale. The method segments the venules and capillaries separately using two parallel branches. It avoids removing capillaries by having very low contrast.

Wang et al. [79] used Hessian-based vessel filtering and fuzzy entropic thresholding. The use of multi-scale allows to segment vessels with various widths. The framework uses a histogram thresholding-based method capable of vessel segmentation by incorporating directional linear information. The fuzzy entropic concepts determine the threshold values.

In [80], preprocessing operations are carried out to improve image segmentation. The approach proposes preprocessing techniques such as the Laplacian operator, homomorphic filtering, and the CLAHE algorithm to enhance the input image. Then the optic disk is removed from the enhanced image, and suitable threshold values are obtained using a threshold technique based on hysteresis with a dynamic T_{High} value obtained from the Otsu method.

Yao [81] proposed a fast 2D-Otsu algorithm by using distributed genetic algorithm based on a migration strategy. The proposed Otsu algorithm can tackle the problem of low contrast in retinal images. The framework combines the Otsu method with PCNN.

Ali et al. [82] used the Frangi filter and Otsu thresholding on the high-boost filtered image to achieve segmentation. The Frangi filter uses a Hessian eigen values-based approach to enhance the vessel's contrast. Their experiments show a detailed comparison of three-vessel segmentation algorithms with different-resolution images.

Table 2
Performance measures, preprocessing and postprocessing techniques to retinal segmentation based on thresholding segmentation methods.

Author	Preprocessing	Technique	Postprocessing	Database	Acc	Sn	Sp
Bahadar et al. [77]	CLAHE, Top-Hat Transform, Hessian Matrix	Otsu	Pixel/area based thresholding	DRIVE STARE	0.9607 0.9458	0.7462 0.7580	0.9801 0.9627
Jiang et al. [78]	Greyscale transform	Top-Hat Transform, Thresholding	Erosion	DRIVE STARE	0.9538 0.9515	0.9159 0.6667	0.9559 0.9813
Dash and Bhoi [85]	Median Filtering, CLAHE	Mean-C	Erosion, dilation	DRIVE	0.955	0.719	0.976
Ozkava et al. [84]	Greyscale Transform, Gaussian and Wiener Filter	Otsu	Morphological operators	DRIVE	0.956	0.85	0.963
Wang et al. [79]	Median filtering, Histogram equalization	Fuzzy entropic thresholding	Threshold selection	DRIVE	–	0.5350	–
Aguirre et al. [83]	Low-pass radius filter	Gabor Filter, fractional Gaussian derivative, threshold	Morphology operators	DRIVE STARE	0.9503 0.9231	0.7854 0.7116	0.9662 0.9454
Mapayi and Owolawi [86]	Median Filtering	Otsu	Morphological Opening and median filter	DRIVE	0.9551	0.7020	0.9796
Ali et al. [82]	Frangi filter	Otsu thresholding	–	DRIVE STARE	0.9889 0.9111	0.6551 0.6577	0.9805 0.8999
Mahapatra et al. [80]	CLAHE, Laplacian Filter, homomorphic filter	Mean Global based on Hysteresis	Morphological Opening	DRIVE	0.9605	0.7035	0.9854

In [83], the authors incorporated fractional Gaussian derivative to a Gabor Filter Bank (GFB). The authors affirm that the combination of these techniques prevents the blurring of the blood vessel borders while keeping the benefits of the Gabor Filter. These two operations allow a thresholding classification rule since they produce a subspace where the samples from each class appear separated.

Ozkaya et al. [84] used G channel and image sharpening to make blood vessels more prominent. The authors use a noise removal process in small steps to avoid being removed from image capillaries. If the noise removal is applied carelessly, the capillaries are damaged, and vessel geometry is disturbed. The authors use the Otsu threshold and morphological operator in the pot processing.

Dash and Bhoi [85] thresholded the images using mean-C thresholding to detect the required blood vessels from the background.

In [86], the authors propose research on the suitability of a multithresholding approach based on Otsu global thresholding technique for the segmentation of retinal vessels.

Due to the variations in the width of the veins, when segmenting the image, the thinnest veins are eliminated as they have very low contrast. It is characteristic of the retinal fundus image. The global thresholding techniques have not been efficient for retinal vessel network segmentation. To tackle this problem, the researchers use a multilevel threshold, a first phase for the venules structure extraction, and a second phase for capillary detection as a complement.

Histogram thresholding-based methods: Typically, a histogram-based image segmentation comprises three stages: Recognizing the modes of the histogram, finding the valleys between the identified modes, and applying thresholds to the image based on the valleys. Some works published in this field cover the peaks detection on the histogram curve based upon homogeneity criteria, recursive thresholding techniques based upon discriminant analysis, maximum correlation criterion for multilevel thresholding, entropy-based, using fuzzy sets, among several others.

One of the simplest and most used methods for segmenting blood vessels in retinal images is thresholding. Pixels are categorized using their intensity levels or other image properties in this type of image segmentation. When the contrast between blood vessels and the background is strong, thresholding techniques work effectively, making it relatively simple to distinguish the two regions. As we reported in Table 2, the most promising method is Otsu, since Otsu's thresholding automatically finds the optimal threshold that minimizes the intra-class variance between vessel and background pixels, maximizing the inter-class variance of pixel intensities. On the DRIVE database, the authors reported models based on Otsu with accuracy, sensitivity, and specificity scores up to 0.98, 0.85, and 0.96, respectively. These values were 0.94, 0.75, and 0.97 on the STARE database. The three preprocessing techniques that are most widely used are CLAHE, Hessian Matrix, and Median Filtering. Additionally, postprocessing techniques including dilatation, erosion, and opening are used.

The main advantages of the thresholding methods are the easy implementation and fast training model. Moreover, the segmentation process is simple in images with high contrast and obtains high precision.

The thresholding methods present problems in images with no significant contrast or overlap of gray scales because threshold methods consider the grayscale, not the spatial information in the image. Also, the noise and the grayscale unevenness are a handicap for the method. In some environments threshold method obtain good results in one image region but not in the rest.

6.2. Tracking based methods

The algorithms of vessel tracking segment vessels are based on manual/automatic selection of local information between two points, seed positions, for a single vessel. This method consists of a vessel containing local centerline information to discover the path of the vessel profile model of best matched and tracking of each vessel with certain properties. This approach gives information about the vessel structure of branching and connectivity; the tracking algorithms do not detect the vessel that is not a seed point, and missing any bifurcation point results in an undetected subtree of an accurate vessel that provides the information about the individual vessel. The advantage of tracking techniques is their competence since only pixels near the preliminary points are analyzed. The disadvantage of this technique is that refined approaches are introduced due to the complex intensity profile at branching or crossover positions. Because vessel bifurcation is poorly modeled, the process often tends to end at these positions, leading to incomplete segmentation. The basic tracking approach is described as follows [87]:

1. Initialization

    - Two initial edge points are selected manually diametrically opposed on the interested blood vessel.

- A central point is chosen, and the initial tracking direction is defined along the local vessel's direction. Iteration

2. Iteration

- Vessel edge points, center point, direction, and diameter are obtained in the previous iteration.
- A search window with a statistical sampling method selects the most probable vessel configuration using Bayesian theory with maximum a posteriori as a criterion. The selection is performed when all the possible configurations with two edge points (normal), four edge points (bifurcation), or six edge points (crossing) are tested.
- The blood vessel parameters such as edge points, direction, and diameter are obtained for the next iteration.
- If the diameter of the blood vessel is less than one pixel, the current vessel's end is found, and the tracking of the current vessel stops.

3. End

- When the vessel branches are found, the algorithm obtains all the initial information about the branches. In this situation, the current tracking process stops, and the tracking of these branches considered new blood vessels, starts.

In [88] is introduced a medial-ness function for the 2D space, which is weighted with a function to reduce the effect of asymmetric structures. The resulting image is multiplied by the eigenvalues of the Hessian matrix at every pixel of the image. Then, a noise reduction from the image background while retaining vascular structures step is applied that uses a formula based on area and elongation. The boundaries of vessels are estimated using eigenvalues and the result of the medialness function. In [89], the vessel contrast is boosted using a 2D Gabor filter. The vessel segmentation obtained using a multilayered thresholding approach traces vessel boundaries and analyzes the connectivity using various thresholds iteratively. It removes all false boundaries and vessel segments before vessel tracking. In [90], was presented a method that combines the bias correction of the intensity inhomogeneity of the retinal image and a matched filter to enhance the appearance of the vessels. The segmentation of the vessels is obtained as a response to the matched filter using the expectation–maximization algorithm. In [91] introduced a self-adaptive matched filter that combines the high sensitivity of the vesselness filter with the high specificity of the matched filter using an orientation histogram. An unsupervised segmentation approach is introduced in [92]; the proposed method provides a basis for the quantitative analysis of large databases. The authors follow an approach of processing image data in a higher dimensional domain, but instead of using the local Radon transform, they rely on the formal group-theoretical framework of orientation scores; besides, a multi-scale approach is applied, using rotation invariant Gaussian derivatives. [93] presented an approach based on a matched filter. The matched filter-based methods compare variations in the intensity level of the cross-section profile of the retinal image with the predetermined template or kernel. The authors statistically analyze the gray scale profile of the retinal images' cross-section data. The extreme values of the probability distribution functions, such are Gumbel, Weibull, and Frechet, are analyzed to design a matched filter kernel of the vessels segmentation. In [94] was introduced a tracking-based method where several seed points are selected automatically on the image, which provides initial parameters for the tracking algorithm. An automatic two-step method based on grid line analysis is used to pick initial seed points. The tracking process starts from each seed point and detects vessel edge points iteratively until the end conditions are satisfied. New vessel edge points are detected using a statistical sampling scheme during the tracking process. A line segment is regarded as a linear search window, which restricts the possible locations of new vessel edge points. The width of the linear window is adaptive to the local vessel diameter to cover the potential positions of new edge points. When all the seed points are processed, all the vascular tress is detected, and the algorithm stops. In [95] was addressed a novel graph-based approach to address tracing with the crossover problem. After the initial segmentation and skeleton extraction, the graph representation is established, where each segment in the skeleton becomes a node, and a direct contact between two adjacent segments is translated to the undirected edge of the corresponding two nodes. The skeleton segments that touch the optical disk area are regarded as root nodes. Determining the number of trees to find in the vessel network equals the number of root nodes. In [96] was proposed an automatic anisotropic fast marching-based geodesic method to extract the centerlines of vessel segments. Every pair of points (from a set of pairs) provides the initial and target points for one geodesic. For each pair of initial and target points, a special Riemannian metric is computed with an additional radius dimension to constrain the marching propagation so the method can get a path without any shortcut. A vessel detection filter obtains The points from a pre-segmented skeletonized image. In [97] presented a curvelet-based method for vessel segmentation, which considers the advantages of both the Jerman filter and curvelet transform for vessels enhancement and mean-C thresholding to improve the performance of the curvelet transform. [98] offered a principled way of addressing the tracing with crossover problem. Local and global contextual information is considered explicitly by connecting to the established algebraic digraph theory and the transductive inference in machine learning.

In [99] was proposed a multi-layer perceptron neural network and the selection of feature vectors. A 24D feature vector is constructed for each image pixel, where information on the local intensity, morphology transformation, principal moments of phase congruency, Hessian, and difference of Gaussian values are encoded. Depending on mathematical morphological operators, a postprocessing technique is employed to optimize the segmentation. The selected feature vectors outfit the symmetric features, providing the final blood vessel probability as a binary map image. [100] presented a combination of techniques, compactness classifier, morphological operator, Gaussian, and thresholding. A function matrix box is added to classify the neovascularization of blood vessels. In [101], presented a scheme based on radial projection and semi-supervised methods. The radial projection method is employed to locate the vessel centerlines, including the low-contrast and narrow vessels. The steerable complex wavelet is modified to provide better capability to enhance vessels under different scales and construct the vector feature to represent the vessel pixel-by-line strength. Semi-supervised self-training is employed to extract the major structures of vessels. In [102] was proposed an edge tracking scheme. This method detects edge points iteratively based on a Bayesian approach using local gray level statistics and continuity properties of vessels. Combining the gray level profile and vessel geometric properties improves the robustness of the tracking process. [103] introduced a tracking approach employing maximum a posteriori probability. The optic disk is detected using analysis of principal components. The Gaussian filter and intensity-gradient co-occurrence matrix segment the retinal vessel. The starting points of vessels are detected around the optic disc. For each vessel, tracking is performed employing Bayesian theory. A semi-ellipse is defined to search a region according to the vessel's width, travel direction, and curvature. There are considered normal vessel, vessel branching, and vessel crossing. In every step, the probabilities of all combinations of candidate points are calculated, and vessel structure and corresponding vessel edge points are determined via Bayesian theory with the maximum a posterior. In [104] was presented a tracking-based method using a probabilistic formulation, and a statistical segmentation scheme is associated with the maximum a posteriori as the criterion to estimate local vessel edges. [105] introduced an automatic algorithm based on a parametric model of a vessel that assumes a complex shape. The vessel tracing algorithm that exploits the geometric model and actively seeks vessel bifurcation without

Table 3
Performance measures, preprocessing and postprocessing techniques to retinal segmentation based on tracking segmentation methods.

Author	Preprocessing	Main algorithms	Postprocessing	Database	Acc	Sn	Sp
Delibasis et al. [105]	–	Geometric vessel model	–	DRIVE	0.9370	0.6731	0.9754
You et al. [101]	Equalization	Radial projection	Morphological operator	DRIVE STARE	0.9434 0.9497	0.7410 0.7260	0.9751 0.9756
Moghimirad et al. [88]	Noise reduction	Multi-Scale vessel medialness detection	Skeletonization	DRIVE STARE	0.9659 0.9756	0.7852 0.8133	–
Yin et al. [94]	–	Statistical sampling, gradient analysis, iterative Bayesian Method	–	DRIVE STARE	0.9267 0.9412	0.6522 0.7248	0.9710 0.9666
Akram and Khan [89]	2-D Gabor	Multilayered thresholding	–	DRIVE STARE	0.9469 0.9502	–	–
Zhang et al. [92]	Luminosity	Gaussian derivatives, Matching	–	DRIVE STARE	0.9446 0.9511	0.7444 0.7940	0.9708 0.9707
Chakraborti et al. [91]	Vesselness filter	Hessian matrix, Matched Filter, Orientation histogram	–	DRIVE STARE	0.9370 0.9379	0.7205 0.6786	0.9579 0.9586
Chen and Cohen [96]	Morphological filters	Constrained Anisotropic Fast Marching	Remove endpoints	DRIVE	0.9397	–	–
Singh and Srivastava [93]	Grayscale transform, CLAHE	Matched filter, optimal thresholding	Length filter	DRIVE STARE	0.9522 0.927	0.7594 0.793	–
Tamim et al. [99]	greyscale transform	Feature extraction	Closing operator	DRIVE STARE	0.9607 0.9632	0.7542 0.7806	0.9843 0.9825
Dash et al. [97]	Jerman Filter	Mean-C thresholding	Morphological operator	DRIVE	0.9600	0.7528	0.9933
Kaba et al. [90]	Bias Correction	Expectation maximization	Length Filter	DRIVE	0.9450	0.6645	–

intervention is described. The proposed algorithm uses the geometric vessel model to determine the vessel diameter at each detected central axis pixel.

Vessel tracking algorithms are used to segment and trace blood vessels in retinal images or other medical imaging modalities. These algorithms typically operate by selecting seed points (initial points) on the vessels and then tracking the vessel's path based on local information in the vicinity of the seed points. The main goal of vessel tracking is to construct the centerline or profile of each vessel accurately. In this section, many tracking-based techniques were discussed. According to Table 3. On the DRIVE database, models based on vessel centerline extraction, Mean-C thresholding, and normalization design of NN testing are the most successful, whereas a model based on vessel centerline is the most successful on the STARE database. The Hessian Filter is also the preprocessing technique that is used the most frequently, and the authors additionally suggested using a variety of postprocessing techniques.

6.3. Region growing

Region-based approaches group the image pixels into clusters, maintaining connectivity among the pixels of the same cluster. In region-based image segmentation, the intensity inside the zone is expected to be roughly constant, to vary only gradually, or to be produced by an appropriate probability model. Region-growing segmentation groups pixels based on how similar they are; the similarity might be shown by differences in intensity, texture, etc. The similarity parameter is defined by a threshold value that adds a neighbor when the difference between the seed pixel and the neighboring pixel is less than or equal to the threshold value. The nearby pixel is grouped with the seed pixel only if the requirement is satisfied, which completes the grouping of related pixels that are a part of the same object.

In [106], the authors preprocessed the images by an adaptive equalized histogram. They used in their experiments the green channel since they considered the channel with the highest contrast between the shapes. They also used the Gabor 2D wavelet technique to improve the image's contrast.

In [107], the authors selected seeds based on Binary Hausdorff Symmetry (BHS). With the proposed method, a binary symmetry is defined in each pixel without the need to calculate the continuous symmetry map and the threshold calculation. In addition to using BHS is designed an edge distance seeded region growth (EDSRG) algorithm with the seeds acquired with the BHS method.

In [108], the authors proposed a method that extracts all blood vessel-like objects using the Laplacian operator technique and removes noisy objects. They define a noisy object when they detect the center lines with the normalized gradient vector field, and each center line is obtained by combining the low-contrast center lines with the high-contrast center lines. High contrast is removed if a low-contrast center line is not close to a center line.

In [109], the authors applied preprocessing by normalization of the background of the images. In their experiments use only the green color channel. Once the preprocessing is done, they perform an enhancement of the bifurcations in the blood vessels, applying line detection filters with four angles (0°, 45°, 90°, and 135°), the difference of Gaussian filters (DoOG) for the selection of candidates of possible lines, the union of each candidate point is performed to identify each segment. Finally, a binary morphological reconstruction is applied, and the segmentation is concluded using the center of the pixels within the lines of the central segment.

In [110], the authors used only the green color space, combining a hysteresis threshold with the similarity of the vector of the adjacent pixels. The authors build a score map to identify possible seeds with the combination of the statistical measures of the response vectors and local maxima. The algorithm performs a segmentation for each vector applied to the images; the two segmentations are merged to build a final binary vascular mask, which will be used for segmentation and useful for thin vessels.

In [111], the authors used growing region and automatic pixel classification. Each classifier is trained with feature vectors extracted from images with real data, including vessel and no-vessel annotation. For the growing region technique, the seeds that are given as the maximum response of applying the Frangi filter is located, and the largest component is chosen according to the connection of the pixels that belong to the vessels. The feature vector to perform pixel classification is given by a Hessian matrix, which is the basis for the Frangi filter for edge detection.

Table 4
Performance measures, preprocessing and postprocessing techniques to retinal segmentation based on region growing segmentation methods.

Author	Preprocessing	Main algorithms	Postprocessing	Database	Acc	Sn	Sp
Martins et al. [112]	Median filter	Maximal Entropic Thresholding Method	Gabor wavelet	DRIVE	–	0.73498	0.9831
Moghimirad et al. [88]	Noise reduction	Multi-Scale vessel medialness detection	Skeletonization	DRIVE	0.9659	0.7852	–
Panda et al. [113]	highboost filtering	Hausdorff Symmetry Operator and k-means	Morphological operators	DRIVE STARE	0.9516 0.9491	0.7380 0.8045	0.9739 0.9606
Zhao et al. [106]	histogram equalization and Gabor wavelet	Anisotropic diffusion filter and Region growing	Remove isolated vessel pixels by logical operations	DRIVE STARE	0.9477 0.9509	0.7354 0.7187	0.9789 0.9767
Lazar and Hajdu [110]	Gaussian Filter	multiscale symmetric matched filter response; two directional response vector maps (DRVMs), the multi-scale symmetric matched filter (MSMF-DRVM) and bottom-hat (BH-DRVM); Region growing	Morphological operators	DRIVE STARE	0.9458 0.9492	0.7646 0.7248	–
Yin et al. [114]	CLAHE, Gabor and wavelet filter	Several region growing	Remove false vessels	DRIVE STARE	0.9506 0.9315	0.8957 0.8886	–
Zhang et al. [115]	Gaussian filter	Gabor filter, SIFT	–	DRIVE	0.9504	0.7812	0.9668
Panda et al. [107]	highboost filtering	Hausdorff distance, Canny edge operator	k-means clustering; SVM	DRIVE STARE	0.9539 0.9424	0.7328 0.8403	0.9752 0.9504
GeethaRamani and Lakshmi [116]	Cropping, Color transformation, Gabor filtering, halfwave rectification	PCA, k-means	Connected Component Analysis, Mathematical Morphological techniques	DRIVE	0.9536	0.7079	0.9778
Khan et al. [117]	Color transformation, Homomorphic filtering	PCA; ISO data extraction algorithm	Multi-Scale line filters	DRIVE STARE	0.9506 0.9513	0.7696 0.7521	0.9651 0.9812
Shukla et al. [118]	Color transformation	Eigenvalue maps	Remove noise by difference eigenvalue maps	DRIVE STARE	0.9476 0.9573	0.7015 0.7023	0.9836 0.9863
Rodrigues et al. [111]	Feature extraction, Connectivity Features	Classifier	Frangi filter, Hessian matrix	DRIVE STARE	0.9740 0.9827	–	–
Lam and Yan [108]	Gaussian filter	Locating the Centerlines Using the Normalized Gradient Vector Field; Detection of Blood Vessel-Like Objects Using Gradient Vector Field	Morphological operators	STARE	0.9474	–	–

The region growing is a segmentation method that divides pixels into regions according to how similar they are. The method begins with a seed pixel or group of seed pixels, and subsequent pixels that satisfy a similarity requirement determined by a threshold value are repeatedly added to the area. Table 4 indicate that models based on Eigenvalue maps, Hausdorff Symmetry Operator, k-means, and PCA obtained the greatest average performance on measures of accuracy, sensitivity, and specificity, when evaluated on the DRIVE and STARE databases. The Gabor wavelet filter and the Gaussian filter, on the other hand, are the most often utilized preprocessing techniques.

The main advantages of the region's growing methods are their flexibility in selecting grow criteria and seed points. This one requires a few seeds to complete the segmentation.

However, its main disadvantages are its high computational complexity and its sensitivity to noise since irregularities in the image can generate gaps and excessive divisions.

6.4. Edge detection based methods

The edge detection methods are one of the widely used approaches to image segmentation. Edge detection methods locate the changes of intensity in the image. A boundary between two pixels with noticeably varying brightness levels is referred to as an edge. These intensity changes correspond to the limits of the objects in the image. The main disadvantages of edge detection techniques are that edge detection methods produce additional borders when images contain a lot of noise or borders, and these techniques cannot easily identify sharp curves. A successful edge-based segmentation regularly has the following steps: Detecting edges, eliminating irrelevant edges, and connecting or grouping. The general procedure is as follows:

1. The image is first smoothed using a Gaussian low-pass filter. This preliminary step is taken to reduce the image noise. Large values of σ will suppress much of the noise at the expense of weakening potentially relevant edges.
2. The local gradient (intensity and direction) is computed for each point in the smoothed image.

$$G(x,y) = \left|G_x(x,y)\right| + \left|G_y(x,y)\right| \tag{69}$$

$$\theta = \tan^{-1}\frac{G_y(x,y)}{G_x(x,y)} \tag{70}$$

3. In a procedure known as no maximum suppression, the algorithm only produces wide ridges, leaving just the pixels at the top of each ridge.
4. The ridge pixels are then thresholded using two thresholds T_{low} and T_{high}: ridge pixels with values greater than T_{high} are considered strong edge pixels; ridge pixels with values between T_{low}

Table 5
Performance measures, preprocessing and postprocessing techniques to retinal segmentation based on Edge detection segmentation methods.

Reference	Preprocessing	Main algorithms	Postprocessing	Database	Acc	Sn	Sp
Orujov et al. [120]	Green channel extraction,Contrast enhancement, Background Exclusion	Fuzzy edge detection	Blood vessels exclusion	DRIVE STARE CHASEDB1	0.939 0.8650 0.9500	0.957 0.8342 0.8800	0.838 0.8806 0.968
Khan et al. [117]	PCA color conversion, Background Homogenization	Iso-data Binarization, Homomorphic filtering, Triple-Stick filtering	–	DRIVE STARE	0.940 0.9513	0.7696 0.7521	0.9651 0.9812
Tchinda et al. [123]	Green channel extraction, Median filter	morphological transformation, Edge detection filters, Multi-Layer Perceptron Strong Contrast remove method	–	DRIVE STARE CHASEDB1	0.9480 0.9548 0.9452	0.7352 0.7265 0.7279	0.9775 0.9759 0.9658
Yang et al. [122]	Histogram equalization	Frangi filtering Local Chan–Vese and Local Binary Fitting models	–	DRIVE STARE	0.9532 0.9476	0.7349 0.7574	0.9743 0.9624
Sigurðsson et al. [124]	CLAHE, Noise reduction	Local minimum and Edge Detection, Path openings	–	DRIVE	0.9455	–	–

and T_{high} are said to be weak pixels. This process is known as hysteresis thresholding.

Edge-based segmentation has several drawbacks, but its main drawbacks are that it performs poorly for images with poorly defined or numerous edges and is more sensitive to noise than other techniques.

Chang et al. [119] described a segmenting retinal blood vessels technique. This method avoids classifying non-vessel pixels as vessel pixels that are very near to the blood vessels. This technique is called Retinal Blood Vessel Segmentation, based on Line and Edge detector. The proposed system works on an inverted green channel image.

In [120] was proposed a contour detection algorithm based on Mamdani (Type-2) fuzzy rules. The method uses the green channel data from eye fundus images as input, CLAHE for contrast enhancement, and a median filter for background exclusion. The Mamdani fuzzy rules applied to image gradient values are used for edge detection.

Toptas and Hanbay [121] proposed a pixel-based feature extraction. The system uses edge detection, morphological, statistical, gradient, and Hessian matrix for feature extraction.

In [122] was proposed a Frangi filter-based multi-scale level sets to segment retinal vessels from fundus images. The proposed approach can deal with the variety of thicknesses in retinal vessels. The author employed histogram equalization to improve the appearance of the retinal images and the outcomes of Frangi filtering and final segmentation. The authors equalize histograms using the CLAHE and Retinex algorithms.

An approach based on edge detection filters and artificial neural networks was proposed in [123]. The features vector is first extracted using edge detection filters. After that, an artificial neural network is trained using the obtained features to determine whether or not each pixel is part of a blood structure. The framework created a features vector to train a cascade feed-forward neural network using edge detection filters like Canny, Sobel, Robert, Prewitt, Laplacian of Gaussian, and morphological filters. According to the researchers, the framework is reliable under a range of luminosity circumstances and vessel widths.

In [124], the feature extraction was performed using advanced morphological directional filter called path openings. The resulting features are used for a data fusion task based on fuzzy set theory. The proposed technique assumes that the vessels are connected linear structures. The method is completely unsupervised and does not need any specific training. According to the authors, the proposed method can isolate major vessels and the majority of smaller vessels with similar or higher accuracy than many other vessel segmentation methods without requiring a significant investment in computer power.

Edge detection methods are used to locate the borders or transitions between several sections or objects in an image. These transitions, which are known as edges, often reflect changes in pixel or intensity values. Edges serve as a representation of an object or structure's boundaries in an image. In summary and as stated in Table 5, models based on Local Chan-Vese (LCV), Local Binary Fitting (LBF), and Multi-Layer Perceptron algorithms showed the best average performance on metrics of accuracy, sensitivity, and specificity. Additionally, Gaussian Filtering and Histogram Equalization are among the most often used preprocessing techniques.

Segmentation methods based on Edge detection are sensitive to image noise and obtain errors in curves, corners, or grayscale intensity variations. Furthermore, these can become computationally very complex.

6.5. Clustering-based methods

Clustering-based methods are one of the most used algorithms in image segmentation. The clustering approaches are used in many different domains of application due to their simplicity and efficacy [125]. The principal disadvantages are that some clustering-based methods require a priori information, particularly the number of clusters, and the algorithms are susceptible to noise and outliers. Fuzzy c-means (FCM) and k-means algorithms are two of image segmentation's most widely used clustering algorithms.

The K-means algorithm is defined in Algorithm 3 [126]:

Algorithm 3 k-means algorithm

Input: Image I, Number of clusters k
Output: Segmented image

1: Initialize cluster centers arbitrarily.
2: For each seed block $n = 1, \ldots, N$, find k given by

$$k = \arg\min_{s} D(A_n, A_s)$$

where s takes values from the set $1, 2, \ldots, k$.
3: Define S_k as the set of seed blocks whose affine parameter vector is closest to $\bar{A}_k$. Then, update the class means $\bar{A}_k = \frac{\sum_{n \in S_k} A_n}{\sum_{n \in S_k}}$
4: Repeat steps 3 and 4 until the class means $\bar{A}_k$ do not change by more than a predefined amount between successive iterations.

Fuzzy c-means algorithm [127] is an important algorithm for image segmentation. A pixel can be a member of multiple clusters in this

iterative clustering technique, and each pixel has a unique set of membership levels assigned to it. The FCM algorithm's process is described in Algorithm 4.

Algorithm 4 fuzzy c-means algorithm

Input: Image I, exponential weight, Number of clusters k
Output: Segmented image

1: Select a number of clusters $2 \leq k \leq n$ and exponential weight $m > 1$
2: Choose an initial partition matrix and a termination criterion ϵ
3: Compute the fuzzy cluster centers $v_i^l, i = 1, 2, \ldots, k$

$$v_i = \frac{1}{\sum_{j=1}^{n} \left(u_{ij}\right)^m} \sum_{j=1}^{n} \left(u_{ij}\right)^m x_j, i = 1, ..., k$$

4: Compute the new partition matrix $\cup^{l+1}$ by using $v_i^l, i = 1, 2, \ldots, k$
5: Compute $\Delta = max_{i,j} \left| u_{ij}^{(} l + 1) - u_{ij}^l \right|$. If $\Delta > \epsilon$, then $l = l + 1$ and go to step 3.
6: If $\Delta \leq \epsilon$, then stop

Several algorithms for retinal vessel segmentation based on clustering have been proposed. In [128], the authors proposed a novel algorithm based on K-means segmentation. The approach improves the segmentation's ability to distinguish between blood arteries and other tissue by lessening the unfavorable effects of light lesions. After removing the bright lesions, the framework uses the multi-scale line detection method. It reduces the possibility of erroneous vessel detection in these areas.

In [129], Mondal et al. used a generalized improved Fuzzy Kohonen Clustering Network (GIFKCN) to segment into vessel and non-vessel clusters. Before using the clustering algorithm, the algorithm uses preprocessing techniques such as CLAHE, Gaussian low pass filter, and morphological operations. All the preprocessing techniques are applied in the green channel.

In [116], the authors used k-means to cluster two groups, namely 'vessel' and 'non-vessel.' In their experiments, the authors use Manhattan's distance to group clusters. The algorithm uses several image preprocessing techniques in some space colors.

In [130], the authors utilized supervised and unsupervised machine learning techniques. The framework uses FCM clustering to extract the thick and clear vessels. The authors use one channel of each space color (G from RGB, L from L*a*b, and Y from YCbCr). It allows to improve the clarity and discriminability of the blood vessels.

In [131] was proposed a novel algorithm to tackle the problem of thin vessel segmentation. The authors use multilevel segmentation and artificial bee colony optimization with fuzzy C-means.

The authors of [132] suggested a matched filtering technique for use with a curvelet transform and kernel-based fuzzy c-means integrated system design platform. The research employs curvelet transform to improve the retinal vasculature. Matched filtering is used to intensify the blood vessels, and the Kernel-based fuzzy c-means technique is utilized to extract the vessel silhouette from the background using non-linear mapping. The system can extract small and thin vessels.

In [133], k-means clustering was employed to classify into vessel and background. Further iterative refinement steps based on morphological operations are applied to refine the segmented image. This method relies on automatic k-means and morphological operator parameter selection. Thus, the algorithm can adapt to different pixel intensity distributions in the image.

In [134], the authors proposed a system based on fuzzy c-means clustering and level sets. The authors equalize the image by contrast-limited adaptive histogram equalization and reduce the noise using mathematical morphology. Matched filtering with Gabor filtering and Frangi filters enhance the blood vessel network before clustering.

Mardani and Maghooli [135] use the density-based spatial clustering of applications with noise (DBSCAN). The authors use morphological operators and logical AND operators to remove noise. The poor contrast and illumination issue, which makes it difficult to segment thin vessels, is a challenge the suggested framework can address.

Clustering-based methods are a group of image segmentation algorithms that classify pixels or areas in an image into clusters based on how similar they are. Contrary to the conventional edge- or region-based segmentation methods, clustering-based methods employ unsupervised learning algorithms to recognize homogeneous groupings of pixels rather than explicit edge or region information. As observed in Table 6, K-means and fuzzy c-means (FCM) were the two key techniques that produced the best results. The most often used preprocessing technique is CLAHE, whereas authors reported employing a variety of postprocessing techniques.

Clustering-based methods are usually straightforward to implement. Furthermore, they can be used on huge sets. However, its main disadvantage lies in the optimal calculation of the number of clusters.

6.6. Methods based on deep learning

Neural networks and deep learning provide the best solutions to many problems in many fields [136–143]. Artificial neural networks are popular machine learning techniques that simulate the mechanism of learning in biological organisms [144–146].

Deep learning represents a keystone of machine learning. It has led to remarkable achievements in problems related to image classification, image segmentation, natural-language processing, autonomous driving, among others .

In recent years, deep learning techniques have been successfully applied to retinal blood vessel segmentation problems because they automatically discover increasingly higher-level features from digital images, Some reviews are presented in [147–149].

This section aims to review the techniques of deep learning state-of-the-art retinal blood vessel segmentation. To do this, we categorize various approaches for retinal vessel segmentation based on their network architecture: Convolutional Neural Network, Fully Convolutional Network, U-Net, and Generative Adversarial Network.

6.6.1. Convolutional neural network

A Convolutional Neural Network (CNN) is a type of deep learning technique used extensively as a powerful class of classification models of digital images in several applications, such as plant species identification, plant disease identification, and retinal vessel detection, among others. A CNN has two main parts: feature learning and classifier. Feature learning extracts visual features from digital images. Then, these features are used by a classifier to determine if an object in the digital images belongs to a specific class.

A CNN is composed of building blocks, such as convolution layers, pooling layers, and fully connected layers. These layers are like feature extractors, dimensionality reduction and classification layers, respectively. These layers of a CNN are stacked to form a full convolutional layer. A general scheme of a CNN is exemplified by Fig. 3.

Retinal blood vessel segmentation influences a lot of blood vessel-related disorders such as diabetic retinopathy, hypertension, cardiovascular and cerebrovascular disorders, among others [150]. In the literature, it is found that vessel segmentation using a CNN showed increased accuracy in feature extraction and vessel segmentation compared to the classical segmentation algorithms. CNN does not need any handcrafted features to train the network classifier. Different approaches that use CNN for retinal blood vessel segmentation have been proposed in the literature, see a performance analysis of the state-of-the-art methods of retinal blood vessels segmentation based on CNNs in Table 7, some of them are described as follows.

In 2016, Maji et al. [152] introduced an ensemble CNN method for processing the fundus color image to get retinal blood vessels. The authors used an ensemble CNN method to reduce overfitting and for validating the method, they used DRIVE database. The method obtained an accuracy of 0.94 and an AUC of 0.92.

Table 6
Performance measures, preprocessing and postprocessing techniques to retinal segmentation based on Clustering segmentation methods.

Reference	Preprocessing	Main algorithms	Postprocessing	Database	Acc	Sn	Sp
Saffarzadeh et al. [128]	Perceptive transform, Greyscale transform	Multi-scale Line operator, K-means clustering, bright reduction	–	STARE DRIVE	0.9438 0.9387	–	–
Hashemzadeh et al. [130]	Image cropping, Color space transformation Color channel selection	Gabor features, FCM clustering	FOV Mask	STARE DRIVE	0.9691 0.9531	0.8087 0.7830	0.9892 0.9800
Memari et al. [134]	Green channel extraction, CLAHE, Color space transform	FCM clustering, Gabor and Frangi filters	morphological operations, Level set refinement	STARE DRIVE	0.9510 0.9610	0.7820 0.7610	0.9650 0.9810
Mardani et al. [135]	Partitioning to cells	DBSCAN, Medfilter, morphological operators	Filter to softens vessels borders	STARE DRIVE	0.9524 0.9519	0.7969 0.7667	0.9664 0.9692
Mondal et al. [129]	(CLAHE) Adaptative equalization, Gaussian filter, Contrast Enhancement	Fuzzy Kohonen Clustering, Morphological operator	–	DRIVE	0.979	0.989	–
GeethaRamani et al. [116]	Image cropping, Color space Transformation, Contrast Enhancement	PCA, K-means clustering, Gabor filtering	Morphology operators	DRIVE	0.9536	0.7079	0.9778
Hassanien et al. [131]	Brightness correction	FCM Clustering	Rank order filtering, Morphological operators	DRIVE	0.9388	0.7210	0.9710
Kar et al. [132]	Green channel, Image denoising, CLAHE	Kernel FCM clustering, Edge enhanced image, LOG kernel	Connected component analysis, Morphological operators	DRIVE	0.9616	0.7548	0.9792
Sun et al. [133]		k-means clustering, morphological thinning algorithm		DRIVE	0.9371	–	–

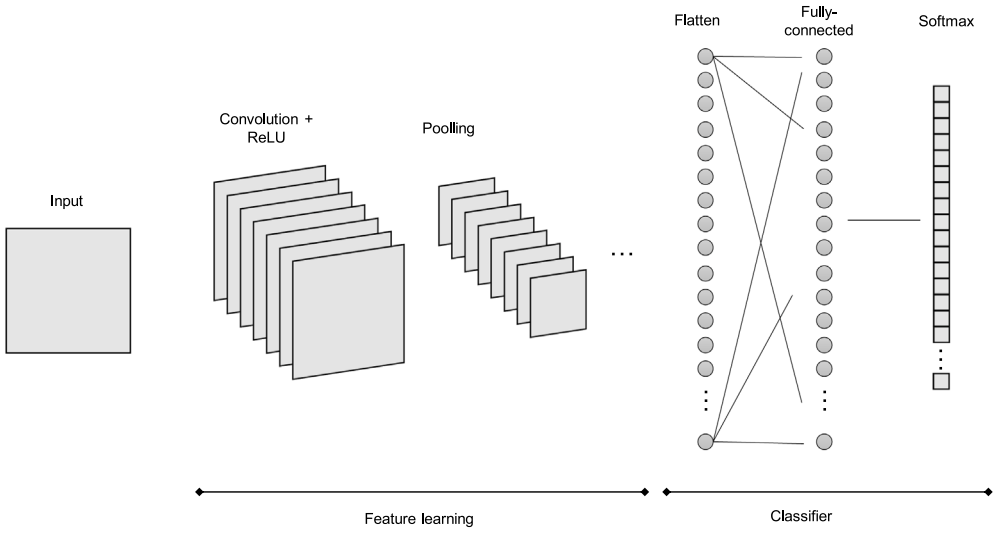

Fig. 3. General scheme of a CNN.

Liskowski and Krawiec [153] proposed a CNN for analyzing retinal blood vessels. The authors employed normalization and ZCA whitening to pre-process the retinal images before the CNN segmentation, they also implemented classifiers based on Naive Bayesian and Nearest-Neighbor to classify the retinal image features. The authors used standard benchmarks of fundus imaging, the DRIVE, STARE, and CHASE_DB1 databases. In their experimental results, the authors reported an ROC curve measure up to 0.99 and accuracy up to 0.97.

Maninis et al. [154] presented a unified framework of retinal image analysis that provides both retinal vessel and optic disc segmentation. The framework is based on CNN called Deep Retinal Image Understanding (DRIU). DRIU uses a base network architecture on which two sets of specialized layers are trained to solve both the retinal vessel and optic disc segmentation. The authors used DRIVE and STARE databases.

Fu et al. [155] formulated a retinal vessel segmentation method for a boundary detection problem, and utilized a CNN architecture to learn the discriminative features that better characterize the important hidden patterns related to vessels and backgrounds in the fundus images. A high-quality vessel probability map is produced to obtain a binary segmentation result by using fully connected Conditional Random Fields segmentation. The authors reported an accuracy of 0.94 and sensitivity of 0.72 on DRIVE database and an accuracy of 0.95 and sensitivity of 0.71 on STARE database.

Wu et al. [156] presented a generic approach for vascular structure identification from medical images based on CNN. The authors trained a CNN model for estimating local vessel probability via PCA and nearest neighbor search, and the resulting map is further utilized within a probabilistic tracking framework to extract the entire connected tree.

Table 7
Overview of approaches using CNNs for retinal image segmentation.

Reference	Preprocessing	Database	Acc	Sn	Sp
Wang et al. [151]	Green channel extraction, Histogram equalization, Gaussian filtering	DRIVE STARE	0.9767 0.9813	0.8173 0.8104	0.9733 0.9791
Maji et al. [152]	–	DRIVE	0.9470	–	–
Liskowski and Krawiec [153]	Extraction of patches, Global Contrast Normalization, Zero-Phase Component Analysis, Data augmentation (scaling, rotation, flipping), Gamma correction	DRIVE STARE	0.9495 0.9566	0.7763 0.7867	0.9768 0.9754
Maninis et al. [154]	Data augmentation (scaling, rotation) and subtract the mean value of the training images for each color channel	DRIVE	0.8121	0.9017	0.6745
Fu et al. [155]	–	DRIVE STARE	0.9470 -	0.7294 0.7140	–
Wu et al. [156]	Extraction of patches	DRIVE	0.9701	–	–
Khalaf et al. [157]	Green channel extraction, Adaptive histogram equalization	DRIVE	0.9456	0.8397	0.9562
Yao et al. [158]	Green component analysis, Extraction of patches	DRIVE	0.9360	0.7731	0.9603
Fu et al. [159]	Extraction of patches	DRIVE STARE CHASEDB1	0.9523 0.9585 0.9489	0.7603 0.7412 0.7130	–
Tan et al. [160]	Green channel extraction, Normalized greyscale image, Convert RGB to LUV color space	DRIVE	–	0.7537	0.9694
Tetteh et al. [161]	–	DRIVE STARE	–	0.8988 0.8389	–
Feng et al. [162]	Extraction of patches, Grayscale transform, Normalization images, Median filter, Adaptive histogram equalization	DRIVE	0.9560	0.7811	0.9839
Soomro et al. [163]	Morphological operations, Grayscale transform, PCA.	DRIVE STARE	0.948 0.947	0.746 0.748	0.917 0.922
Ngo and Han [164]	Max-resizing technique	DRIVE	0.9533	0.7464	0.9836
Guo et al. [165]	Extraction of patches	DRIVE STARE	0.9199 0.9220	–	–
Jiang et al. [166]	–	DRIVE STARE CHASEDB1	0.9709 0.9781 0.9721	0.7839 0.8249 0.7839	0.9890 0.9904 0.9894
Samuel et al. [150]	Contrast Limited Adaptive Histogram Equalization, Gamma correction	DRIVE STARE HRF	0.9609 0.9646 –	0.8282 0.8979 0.8655	0.9738 0.9701 –
Yang et al. [167]	Data augmentation, CLAHE algorithm	DRIVE	0.951	0.797	0.973
Hua et al. [168]	Patches augmentation	DRIVE	0.9511	0.7932	0.9741
Noh et al. [169]	Zero-score normalization, data augmentation (rotation, random brightness modification, contrast modification, random color enhancement)	DRIVE STARE CHASEDB1	0.9569 0.9764 0.9778	0.9746 0.9864 0.9871	0.8354 0.8537 0.8523
Yu et al. [170]	Extraction of patches, zero-phase component analysis, global contrast normalization	DRIVE STARE	0.9524 0.9613	07643 0.7837	0.9803 0.9822
Uysal and Guraksin [171]	Grayscale transform, CLAHE, Gamma correction	DRIVE STARE	0.9419 0.9471	.07548 0.7377	0.9682 0.9735
Xu et al. [172]	Grayscale transform, Gaussian filter, local histogram equalization, Gamma correction	DRIVE STARE	0.9590 0.9688	0.8320 0.8295	0.9885 0.9785
Chala et al. [173]	Data augmentation (rotation, flip or mirroring), Green channel representation	DRIVE STARE	0.9645 0.9707	0.7982 0.7858	0.9840 0.9884
Xia et al. [174]	Gray level transformation, Z-score Normalization, CLAHE, Extraction of patches	DRIVE STARE CHASEDB1	0.9621 0.9715 0.9702	0.8090 0.8384 0.7849	0.9804 0.9832 0.9872
Xu and Fan [175]	2D Gabor filter, CLAHE	DRIVE CHASEDB1	0.9630 0.9604	0.8745 0.8916	0.9823 0.9794
Vengalil et al. [176]	Extraction of patches, No preprocessing	HRF	0.9394	–	–
Mahapatra et al. [177]	Saliency algorithm, Gray level transformation	DR screening initiative	0.979	0.982	0.978

The authors validated their approach on DRIVE database achieving an AUC of 0.97.

Khalaf et al. [157] proposed a seven layers CNN to capture different patterns of retinal vessels as well as enhance the localization of segmentation vessels. To enhance the vessels before the segmentation, adaptive histogram equalization followed by top hat filtering is applied to the green channel of every image. The authors reported accuracy of 0.9456 on DRIVE database.

Yao et al. [158] proposed a method based on CNN to extract blood vessels from fundus images. The proposed method separates each pixel in the retinal fundus image into foreground and background. The foreground represents blood vessels. Segmentation of retinal fundus image is refined by a two stages binarization and a morphological operation. The method was tested on DRIVE database obtaining 0.96 of specificity, 0.77 of sensitivity, and 0.93 of accuracy.

Vengalil et al. [176] presented a blood vessel segmentation method based on CNN. The CNN consists of 8 convolutional layers and 3 pooling layers in between. The authors used a pre-trained model, DEEPLAB-COCO-LARGEFOV, from COCO. The model was fine-tuned using training images consisting of image patches of size 512 × 512 extracted from high-resolution fundal images along with corresponding ground truth. The method obtained an accuracy of 0.93 and a ROC curve of 0.894 on HRF database.

Fu et al. [159] solved the retinal vessel segmentation problem using a CNN architecture called DeepVessel. The proposed CNN architecture consists of 3 main layers. The first is a convolutional layer used to learn a multi-scale discriminative representation. The second is a side-output layer that operates with the early layers to generate a companion local output. The last one is a CRF layer, which is employed to further take into account the non-local pixel correlations. The author used three public databases: DRIVE, STARE, and CHASE_DB1. In all databases, the method obtained more than 0.94 of accuracy and 0.71 of sensitivity.

Mahapatra et al. [177] proposed a method for retinal image quality assessment (IQA) that uses computational algorithms imitating the

working of the human visual system. The authors used a local saliency map that calculates saliency values for every image pixel across different scales, and captures local and global image information that is relevant for IQA; they also used CNN to extract additional information thus avoiding hand-crafted features. Finally, they combined supervised (trained CNN) and unsupervised (local saliency maps) models using Random forest (RF) classifiers. The authors used a database acquired from a diabetic retinopathy screening initiative.

In 2017, Tan et al. [160] presented a method based on CNN constituted by 7 layers and the output layer consists of 4 neurons, representing background, optic disc, fovea and blood vessels. The proposed method not only detects the retinal blood vessels but also the optic disc and fovea of the retinal image. On average, the segmentation correctly classified 0.92 of the ground truths (on the testing set from DRIVE database). The highest accuracy achieved on a single image was 0.94 and the lowest was 0.88.

Tetteh et al. [161] proposed a feature extraction scheme based on inception CNN models for pixel classification tasks. The authors extracted features under multi-scale and multi-layer schemes through convolutional operators. The model was tested using DRIVE and STARE databases obtaining precisions of 0.80 and 0.81, respectively.

Feng et al. [162] presented a patch-based fully CNN with skip connections for blood vessel segmentation. The proposed CNN learns hierarchical features and context information from raw pixel data without any prior domain knowledge. The proposed method obtained an accuracy of 0.95 on DRIVE database.

Soomro et al. [163] developed a CNN model for retinal vessel segmentation to address the issue of low sensitivity. The authors used a pre-processing step on data based on morphological tactics and the color-to-grey conversion-based PCA tactics. Then, they trained a CNN model on the preprocessed data to get an initial good vessel image. The model was tested on DRIVE and STARE databases with a sensitivity of 0.75.

Ngo and Han [164] proposed a novel max-resizing technique to improve the generalization of the training procedure for predicting blood vessels from retinal fundus images. To do this, the authors developed a multi-level CNN model applied for automatic blood vessel segmentation. The proposed network has two input branches with different resolution input images and the max-resizing technique is used for reducing the resolution of the input image in the second branch of the network which increases generalization of the training course. The technique obtained an accuracy of 0.95 on DRIVE database.

Guo et al. [165] proposed a retinal vessel detection approach. To do this, the authors formulated the detection task as a classification problem and solve it using a CNN as a two-class classifier. The CNN architecture has 2 convolution layers, 2 pooling layers, 1 dropout layer, and 1 loss layer. The main parts of this approach are: a new model of CNN to extract features and classify the retinal vessel region and a novel reinforcement sample learning scheme that was used to train the CNN with fewer iterations of epochs and less training time. The proposed method obtained an accuracy of 0.91 on DRIVE database and an accuracy of 0.92 on STARE database.

Hu et al. [178] proposed a novel retinal vessel segmentation method by combining multiscale CNN with an improved loss function and CRFs to detect more details and hard examples. The authors divided the segmentation process into two steps. Firstly, a multiscale CNN architecture with an improved cross-entropy loss function is proposed to produce the probability map from image to image. Secondly, CRFs are applied to get the final binary segmentation result which makes use of more spatial context information among all of the pixels in the fundus images. The authors reported accuracy of 0.95 on DRIVE database and an accuracy of 0.96 on STARE database.

Yu et al. [170] presented a framework for hierarchical division of retinal vascular networks. Specifically, in the first stage, a supervised segmentation technique based on CNN is used for blood vessel segmentation. The authors also presented 2 algorithms: the potential landmark detection algorithm (PLDA) to identify the bifurcations and crossings; and the adaptive hierarchical classification algorithm (AHCA) that is used in the hierarchical characteristics classification of vascular bifurcations. The proposed framework achieved an accurate rate of 0.9899 and a sensitivity rate of 0.9217 on STARE database.

Uysal and Guraksin [171] proposed a hybrid method based on CNN architectures and image processing techniques for segmentation of blood vessels in retinal images. The authors use four-step image processing techniques to significantly extract blood vessels from the background and to standardize retinal images for the training of the CNN model. The authors reported accuracies of 0.9419 and 0.9471 on DRIVE and STARE databases, respectively.

Chala et al. [173] proposed an end-to-end method for automatic features learning from CNN model based on multi-encoder–decoder architecture and building feature maps to get the output as the segmentation of retinal blood vessels. The proposed model-based CNN consists of 4 main components: 2 encoder units (RGB and green encoder), a decoder, and a module for progressive dimension reduction to obtain the retinal vessel segmentation. The authors tested their method by combining DRIVE and STARE databases. The values obtained for the different metrics F1 score, accuracy, sensitivity, specificity, and precision were 0.8321, 0.9716, 0.8214, 0.9860, and 0.8466 respectively.

Xu et al. [172] presented a novel retinal vessel segmentation method based on a residual convolution neural network. The proposed method involves three major components: the residual learning is introduced in the network structure; the atrous spatial pyramid pooling is built to learn the feature information of different receptive fields; the residual attention module and deep supervision module are applied to improve the accuracy of identifying the capillaries. The method was tested on DRIVE and STARE databases obtaining accuracies of 0.9590 and 0.9688, respectively.

Alvarado-Carrillo and Dalmau-Cedeño [179] proposed a novel Width Attention-based Convolutional Neural Network, called WA-Net. The WA-Net works as follows, a fundus image is decomposed into multiple channels by a layer of Distorted Second-Order Differential Gaussian Matched Filters (DSD-GMF). Subsequently, the channel relevance is weighted through the Width Attention Module (WAM). Finally, to specialize the feature maps with a concrete vessel-width category, either thin-vessel or thick-vessel related, the weighted channels are divided into two groups by the Two-Stream Block, composed of three-level UNet streams. The authors reported accuracies of 0.9575, 0.9665, and 0.9653 on DRIVE, STARE, and CHASE_DB1 databases, respectively.

Xia et al. [174] proposed a hierarchical recurrent convolution neural network called HRNet. HRNet integrates SE-residual block in multi-scale layers that capture the important channel-wise information and remove the redundant feature in deep network. Moreover, the authors designed a hierarchical recurrent(feedback) mechanism to explore features from different upper to lower layers by adding the output of each layer to its corresponding encoding layer iteratively.

Xu and Fan [175] developed a retinal vessel segmentation method based on a dual-channel asymmetric CNN. The proposed method is based on the preprocessing of orientation and scale features of retinal images. An asymmetrical CNN, MainSegment-Net, and FineSegment-Net, are constructed in the proposed method according to the characteristics of thick and thin vessels. The segmentation results of the two channels are fused to achieve complementarity of detailed information. The method obtained an accuracy of 0.9677 on DRIVE database.

Despite the great success of CNNs in finding strong spatially local correlations on databases of retinal blood images at different abstraction levels, one of the main problems of using typical CNN for segmenting vessels is the need to divide a given image into a very large number of small patches and classify each of them, causing a high computational cost [180]. On the other hand, a fully-connected layers force all the input images to have the same size.

The main advantages of CNNs are that they can be implemented in a wide range of applications, they also have an excellent capacity

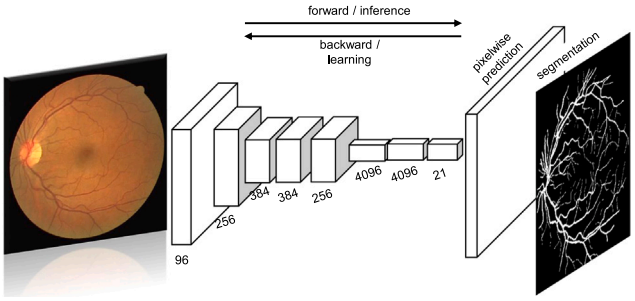

Fig. 4. A FCN scheme for retinal vessel segmentation.

for generalization, and an enormous ability to learn patterns almost without human interference. However, their main disadvantage lies in the need for a large number of images during the training phase, in addition to computational requirements such as a large amount of memory, CPU, and graphics card, in addition to the enormous training time in some cases.

6.6.2. Fully convolutional network approaches

To address the limitations of CNN architectures, one of the leading deep learning techniques for image segmentation and dense prediction is the Fully Convolutional Network (FCN) proposed by Long et al. [181] in 2014. The FCN architecture consists of convolutional layers without using fully-connected layers. This allows the segmentation image to be generated from any input image with an arbitrary size (making this design much more adaptable to different imaging conditions). Moreover, an FCN uses ground truth as supervision information to train the network for pixel-level prediction, thereby further extending image-level classification to pixel-level classification. An FCN scheme for retina vessel segmentation is illustrated in Fig. 4. Many approaches that use FCN have been proposed to address retinal vessel segmentation, see Table 8.

Luo et al. [182] presented a novel Size-Invariant Fully Convolutional Neural Network (SIFCN) to extract retinal blood vessels from retinal images. The authors introduced a patch-wise retinal image segmentation approach that considers more context information during segmentation. The network results in an average accuracy of 0.9471 and an average AUC of 0.968 on DRIVE database.

Dasgupta and Singh [183] presented a fully convolutional neural network architecture for blood vessel segmentation. The authors formulated the vessel segmentation problem as a multi-label inference problem which is learned by joint loss function. The main contribution of this work was to combine the advantage of a fully convolutional neural network and a structured prediction approach for retinal blood vessel segmentation in fundus images. The proposed network was tested on DRIVE database obtaining an accuracy of 0.95.

Jiang et al. [184] developed a supervised method to segment retinal blood vessels from the retinal color images using a pre-trained CNN model. The proposed method has innovatively simplified and shifted a typical retinal vessel segmentation problem into regional semantic vessel element segmentation tasks, in this way the training data has been ideally augmented. The method was tested on DRIVE, STARE, CHASE_DB1, and HRF databases.

Oliveira et al. [185] proposed a method that combines Stationary Wavelet Transform for multiscale analysis and a multiscale Fully Convolutional Neural Network to cope with the varying width and direction of the vessel structure in the retina. Furthermore, the authors used data augmentation (rotations). The authors reported an average accuracy of 0.9576, 0.9694, and 0.9653 on DRIVE, STARE, and CHASE_DB1 databases, respectively.

Lyu et al. [187] proposed a novel retinal vessel segmentation method using Separable Spatial and Channel Flow and Densely Adjacent Vessel Prediction to capture maximum spatial correlations between vessels. The authors used geometric transformations and overlapped patches in the training and prediction phases. The authors reported areas under the ROC curve of 0.9826 and 0.9865 and the average accuracies of 0.9579 and 0.9664 on DRIVE and CHASE_DB1 databases, respectively.

Araújo et al. [180] developed an FCN to segment an unseen image at a single step, even if it is trained in a patch-wise fashion. The authors reported accuracies of 0.956, 0.965, and 0.965 on DRIVE, STARE, and CHASE_DB1 databases, respectively.

Khan et al. [190] presented an encoder–decoder based FCN architecture for vessel segmentation called VessSeg. VessSeg consists of 13 convolutional layers similar to the VGG16 network and a corresponding decoder network. The output of the final decoder in the decoder network is fed to a two-class softmax classifier for pixel-wise classification. The output of the softmax classifier is pixel probabilities which categorize pixels either belonging to the vessel or the non-vessel class. The detection accuracy was significantly improved with scores of 0.9620, 0.9623, and 0.9620 on DRIVE, STARE, and CHASE_DB1 databases, respectively.

Park et al. [194] developed a conditional generative adversarial network called M-GAN for retinal vessel segmentation by balancing losses through stacked deep FCN. This approach consists of a newly designed M-generator with deep residual blocks for more robust segmentation and an M-discriminator with a deeper network for more efficient training of the adversarial model. The authors reported accuracies of 0.9706, 0.9876, 0.9763, and 0.9761 on DRIVE, STARE, CHASE_DB1, and HRF databases, respectively.

Sathananthavathi et al. [188] developed a parallel fully convolved neural network-based architecture for retinal blood vessel segmentation. The ideas of this work are that thin vessel detection is incorporated with the help of parallel fully convolutional architecture. The illumination and contrast non-uniformity effect can be reduced with the help of preprocessing processes. The authors reported accuracy of 0.9637, a sensitivity of 0.8653, and a specificity of 0.9818 on DRIVE and STARE databases.

Khan et al. [191] proposed a reduced FCN (in terms of the number of parameters) called RC-Net to vessels segmentation. RC-Net has 6 convolutional blocks, where the first block of these is the input one, followed by two down-sampling convolutional blocks. There is an intermediate convolutional block that bridges between the down and upsampling blocks. There are 2 up-sampling convolutional blocks followed by the final convolutional output block which is equipped with the essential final layers responsible for creating the pixel-wise segmentation map. RC-Net was tested on DRIVE and STARE databases obtaining accuracies of 0.9694 and 0.9761, respectively.

Atli and Gedik [192] proposed an FCN for retinal blood vessel segmentation called Sine-Net. Sine-Net model first up-samples before down-sampling to capture thin and thick blood vessel features. Furthermore, the method includes residuals to carry more contextual information to the deeper levels of the architecture. The authors combined DRIVE, STARE, and CHASE_DB1 databases, called cross-database training. The proposed Sine-Net model obtained an accuracy of 0.9686.

Samuel and Veeramalai [193] presented a novel CNN model for extracting retinal blood vessels from both the coronary angiogram and the retinal fundus images using a single VSSC Net after performing the image-specific preprocessing. The VSSC Net is composed of the base VGG-16 and two-vessel extraction layers. Each of the vessel extraction layers uses VSC blocks, SC layers, and feature map summation with added supervision. The model was tested on DRIVE, STARE, CHASE_DB1, and HRF databases.

Table 8
Overview of approaches using FCNs for retinal image segmentation.

Reference	Preprocessing	Database	Acc	Sn	Sp
Luo et al. [182]	Green channel analysis, Extraction of patches	DRIVE	0.9536	0.7508	–
Dasgupta and Singh [183]	Green channel extraction, CLAHE, Gamma correction	DRIVE	0.9533	0.7691	0.9801
Jiang et al. [184]	Otsu's threshold, Gaussian filter, Data augmentation (flipping, rotation, scaling, and cropping)	DRIVE	0.9624	0.7540	0.9825
		STARE	0.9734	0.8352	0.9846
		CHASEDB1	0.9668	0.8640	0.9745
		HRF	0.9650	0.8010	0.8010
Oliveira et al. [185]	Stationary Wavelet Transform, Extraction of patches	DRIVE	0.9576	0.8039	0.9804
		STARE	0.9694	0.8315	0.9858
		CHASEDB1	0.9653	0.7779	0.9864
Jiang et al. [186]	Grayscale transform, CLAHE, Gamma correction	DRIVE	0.9706	0.8325	0.9838
		STARE	0.9777	0.8522	0.9880
		CHASEDB1	0.9773	0.8453	0.9862
Lyu et al. [187]	Green and Red channel analysis, Data augmentation (rotation), Extraction of patches	DRIVE	0.9579	0.7940	0.9820
		CHASEDB1	0.9640	0.7878	0.9865
Araújo et al. [180]	Extraction of patches, no preprocessing	DRIVE	0.9560	0.8030	0.9790
		STARE	0.9650	0.8290	0.9800
		CHASEDB1	0.9650	0.8210	0.9810
Sathananthavathi et al. [188]	Green channel analysis, CLAHE, Opening operation, Gaussian filters	DRIVE	0.9637	0.8653	0.9725
Soomro et al. [189]	Morphological tactics, PCA, Gray level transformation,	DRIVE	0.9560	0.8700	0.9850
		STARE	0.9680	0.8480	0.9860
		CHASEDB1	0.9760	0.8860	0.9820
		HRF	0.9620	0.8290	0.9620
Khan et al. [190]	–	DRIVE	0.9620	0.8255	0.9760
		STARE	0.9623	0.8318	0.9758
		CHASEDB1	0.9620	0.8291	0.9730
Khan et al. [191]	–	DRIVE	0.9694	0.8319	0.9826
		STARE	0.9761	0.8427	0.9870
Atli and Gedik [192]	Operations for the noisy images	DRIVE	0.9689	0.7987	0.9854
		STARE	0.9682	0.6574	0.9933
		CHASEDB1	0.9676	0.7876	0.9892
Samuel and Veeramalai [193]	Green channel analysis, CLAHE, Gaussian filter	DRIVE	0.9627	0.7827	0.9821
		STARE	0.9737	0.8738	0.9812

6.6.3. U-net architecture for retinal vessel segmentation

Recently, one of the most popular deep learning architectures for the segmentation of biomedical images is U-Net [195]. The U-Net architecture consists of an encoder that extracts spatial features from an image and a decoder that uses the encoded features to construct a segmentation feature map, the U-Net architecture is shown in Fig. 5. In particular, U-Net architecture combines traditional convolutional layers with upsampling to learn both local and global features. Therefore, U-Net and its extensions have achieved great state-of-the-art results, see Table 9.

Yang et al. [220] proposed a hybrid method to improve the vessel segmentation precision of fundus images. The method performs feature extraction simultaneously for both thick and thin vessels to enhance the correlation between these two vessels under different segmentation networks. An improved U-net network is proposed to act as the basic network of the multitask segmentation network, and an effective loss function is designed to adapt to two different vessel segmentation tasks to solve the imbalanced ratio between thick vessels and thin vessels. The proposed method obtained accuracies of 0.9579, 0.9821, and 0.9776 on DRIVE, STARE, and CHASE_DB1, respectively.

Wu et al. [222] proposed ARU-Net, a deep learning model to automatically segment retinal blood vessels in fundus images. The model leverages the strengths of U-Net, cascaded atrous convolution, and residual blocks enriched with squeeze and excitation. Residual blocks are used as building units to simplify the training process and help extract coarse and fine features from source images. Squeeze and excitation units are added to each remaining block for channel attention, adaptive feature recalibration, and increased feature power representation. The addition of a dilated convolution module can ensure global and multi-scale extraction. The authors reported accuracies of 0.96 and 0.97 on DRIVE and CHASE_DB1, respectively.

Zhang et al. [223] studied the vessel terminals of the retinal vascular branches. To do this, the authors presented new edge-aware flows into U-Net encoder–decoder architecture to guide the retinal vessel segmentation. The authors reported accuracies of f 0.9701, 0.9691, and 0.9811 on DRIVE, STARE, and CHASE_DB1, respectively.

Zhang et al. [224] proposed a deep network architecture named Bridge-net to make use of the context of the retinal blood vessels efficiently. Bridge-net combines an RNN into a CNN to deliver the context and then produce the probability map of the retinal blood vessels. The authors introduced a patch-based loss weight mapping to correct the imbalance of the image. The authors reported accuracies of 0.96668, 0.9834, and 0.9667 on STARE, DRIVE, and CHASE_DB1, respectively.

Dong et al. [226] proposed a cascaded residual attention U-Net called CRAUNet to analyze coarse-to-fine retinal vessel segmentation. The authors also presented a DropBlock regularization to reduce overfitting problem and a multi-scale fusion channel attention (MFCA) module. The CRAUNet obtained AUC of 0.9830 and 0.9865 on DRIVE and CHASE_DB1 databases.

U-Net-based methods, proposed in the literature, have been successfully used in retinal vessel segmentation tasks, but there are still some obstacles that require an in-depth examination and analysis, such as the loss of microvasculature details at the end of vessels, preservation of capillaries, vascular structures of complex bifurcation, the false recognition of the lesion area, the fracture of the small vessel segmentation, a noisy environment (without any additional processing), the impact of loss function selection, among others [227–232].

6.6.4. Generative adversarial network for retinal vessel segmentation

Generative Adversarial Network (GAN) [233] is a type of deep unsupervised generative model, which consists of two network models: generator G for creating new synthetic images (data distribution), and discriminator D for distinguishing human-annotated vessel maps (real label) or machine-generated vessel maps (fake label), see general scheme in Fig. 6. Many researchers used GANs to address the critical limitation of a few images available for training and the imbalance problem, see Table 10.

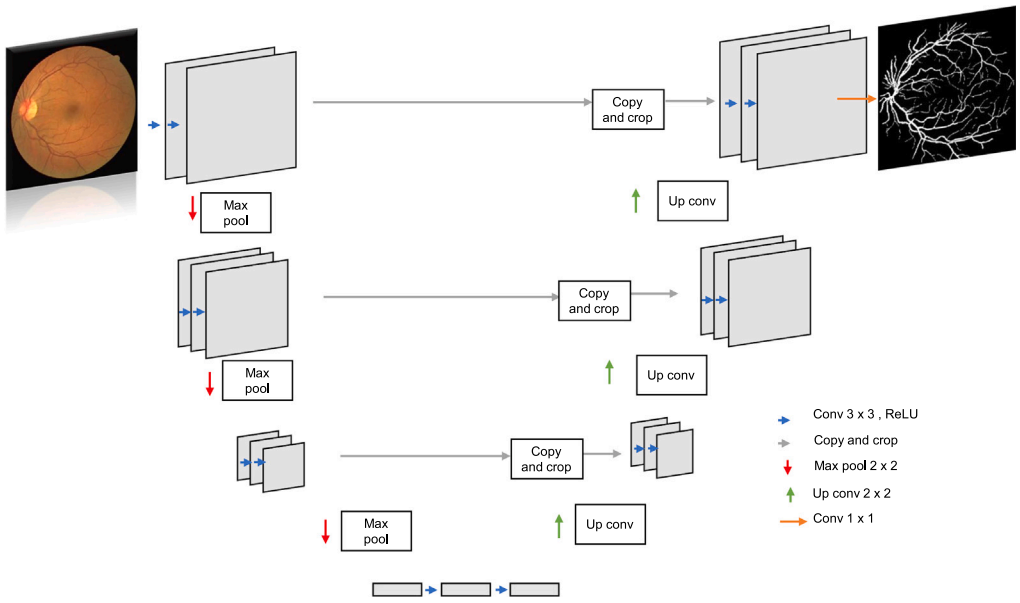

Fig. 5. The U-Net architecture scheme.

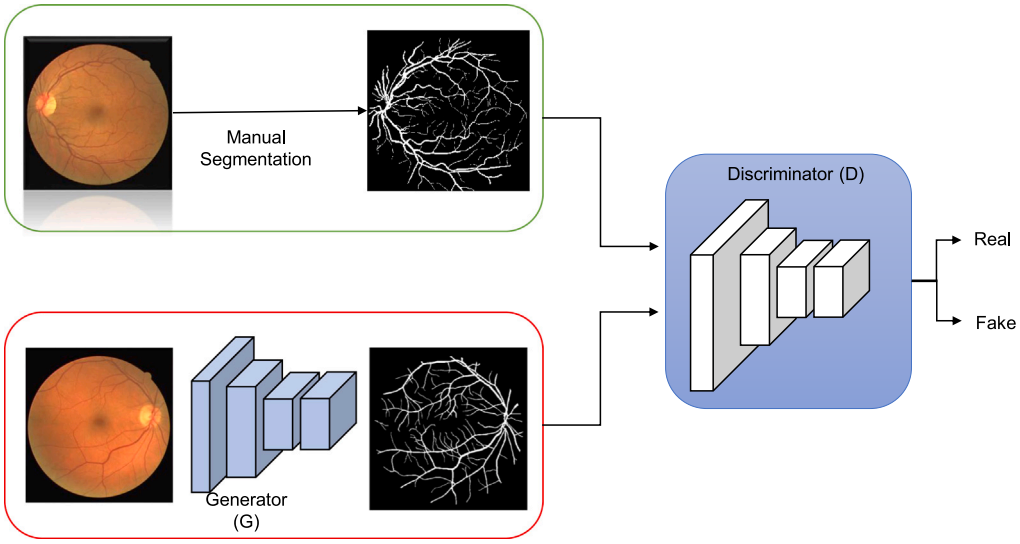

Fig. 6. General GAN scheme.

Park et al. [194] developed a conditional generative adversarial network called M-GAN for retinal vessel segmentation by balancing losses through stacked deep FCN. This approach consists of a newly designed M-generator with deep residual blocks for more robust segmentation and an M-discriminator with a deeper network for more efficient training of the adversarial model. The authors reported accuracies of 0.9706, 0.9876, 0.9763, and 0.9761 on DRIVE, STARE, CHASE_DB1, and HRF databases, respectively.

Zhou et al. [241] presented a method for retinal vessel segmentation on elusive vessels in low-contrast background and lesion regions. To do this, the authors developed a symmetric equilibrium generative adversarial network (SEGAN) that used the characteristics of U-Net and Generative Adversarial Network (GAN). Furthermore, they presented the multi-scale feature refine blocks (MSFRB) to merge the different scale features. MSFRB preserves high-resolution features with high-semantic ones simultaneously.

Zhao and Feng [242] proposed a GAN-based deep network with residual module and attention called Deep Att-ResGAN. The network consists of 4 identical subnetworks. The output of each subnetwork is imported to the next subnetwork as contextual features that guide the segmentation. Deep Att-ResGAN was tested on DRIVE and STARE databases. The authors reported accuracies of 0.9565 and 0.9690, respectively.

Yang et al. [243] introduced a method that combines GAN and end-to-end network generation. The method can distinguish between global and local perception domains through a multi-scale CAM discriminator, and the generator can also use linear attention to transform more efficient blood vessel segmentation. The author reported accuracy of 0.9559 on DRIVE database.

Liang et al. [250] proposed an end-to-end conditional generative adversarial network with class feature loss and improved retinal detail loss, which takes the vessels and masks of retinal images as conditions, aiming to learn rich physiological information contained in fundus images by the end-to-end way and generate high-quality retinal images. The authors used FID metric to measure the similarity between the generated image and the real image in terms of global features, and

Table 9
Overview of approaches using U-Net for retinal image segmentation.

Reference	Preprocessing	Database	Acc	Sn	Sp
Li et al. [196]	Data augmentation (Shifting, rotation, disturb the image with the Gaussian noise), Normalized mean	DRIVE	0.9394	0.8574	0.8231
Gao et al. [197]	Green channel analysis, CLAHE, Gaussian matched filter	DRIVE	0.9636	0.7802	0.9876
Wang et al. [198]	Grayscale transformation, CLAHE, Gamma correction	DRIVE	0.9581	0.7991	0.9813
		STARE	0.9673	0.8186	0.9844
		CHASEDB1	0.9670	0.8239	0.9813
		HRF	0.9654	0.7803	0.9843
		IOSTAR	0.9652	0.7538	0.9893
		RC-SLO	0.9699	0.8681	0.9797
Li et al. [199]	–	DRIVE	0.9568	0.7921	0.9810
		STARE	0.9678	0.8352	0.9823
		CHASEDB1	0.9635	0.7818	0.9819
		IOSTAR	0.9544	0.7322	0.9802
		RC-SLO	0.9696	0.8452	0.9807
Mostafiz et al. [200]	Green channel analysis, CLAHE, Gaussian filter	DRIVE	0.9675	0.7690	0.9865
		STARE	0.9537	0.7689	0.9862
Soomro et al. [201]	Morphological tactics, PCA	DRIVE	0.948	0.739	0.956
		STARE	0.9470	0.7480	0.9620
Luo et al. [202]	Data augmentation (rotation, randomly add noise)		0.865	–	–
Alom et al. [203]	Extraction of patches	DRIVE	0.9556	0.7792	0.9813
		STARE	0.9712	0.8298	0.9862
		CHASEDB1	0.9634	0.7756	0.9820
Xu et al. [204]	Histogram matching	DRIVE	0.832	0.870	0.980
Galdran et al. [205]	–	DRIVE	0.9567	–	–
Yan et al. [206]	Green channel analysis, Extraction of patches, Data augmentation (flipping, rotation, resizing, adding random noise)	DRIVE	0.9542	0.7653	0.9818
		STARE	0.9612	0.7581	0.9846
		CHASEDB1	0.9610	0.7420	0.9809
Zhang and Chung [207]	CLAHE, Extraction of patches, Data augmentation	DRIVE	0.9504	0.8723	0.9618
		STARE	0.9712	0.7673	0.9901
		CHASEDB1	0.9770	0.7670	0.9909
Wang et al. [208]	Grayscale transform, Normalization, Data augmentation, Extraction of patches	DRIVE	0.9511	0.7986	0.9736
		STARE	0.9538	0.7914	0.9722
Luo et al. [209]	Grayscale transform, CLAHE, Green channel analysis	DRIVE	0.9663	0.8075	0.9814
		STARE	0.9684	0.8437	0.9762
Soomro et al. [210]	Fuzzy C-Mean, CLAHE	DRIVE	0.9590	0.8020	0.9740
		STARE	0.9610	0.8010	0.9690
Jin et al. [211]	CLAHE, Gamma correction	DRIVE	0.9566	0.7963	0.9800
		STARE	0.9641	0.7595	0.9878
		CHASEDB1	0.9610	0.8155	0.9752
		HRF	0.9651	0.7464	0.9874
Biswas et al. [212]	Grayscale transform, CLAHE, gamma correction	DRIVE	0.9561	0.7823	0.9814
Ding et al. [213]	CLAHE, Gamma adaptive correction	DRIVE	0.9611	–	–
		STARE	0.9962		
Cheng et al. [214]	Grayscale transform, Z-score standardization, CLAHE, Gamma correction	DRIVE	0.9559	–	–
		CHASEDB1	0.9488		
Tang et al. [31]	CLAHE, Gamma correction	DRIVE	0.9551	0.9682	–
		STARE	0.9687		
Mou et al. [215]	Data augmentation (rotation, random contrast enhancement)	DRIVE	0.9594	0.8126	0.9788
		STARE	0.9685	0.8391	0.9769
		CHASEDB1	0.9637	0.8268	0.9773
Reyes-Figueroa and Rivera [216]	Grayscale transform, Normalization, CLAHE, Gamma correction	DRIVE	0.9515	0.8400	0.9622
		STARE	0.9342	0.8435	0.9531
Chen et al. [217]	Extraction of patches	DRIVE	0.9552	0.8211	0.9748
		STARE	0.9699	0.8466	0.9822
		CHASEDB1	0.9642	0.8395	0.9766
Sun et al. [218]	Extraction of patches, Data augmentation (flipping, rotation, shifting)	DRIVE	0.9671	–	–
		STARE	0.9714		
		CHASEDB1	0.9751		
Alvarado-Carrillo et al. [219]	Quantum convolutional layer, Distorted Gaussian matched filter	DRIVE	0.9772	0.7960	0.9799
		STARE	0.9837	0.7904	0.9843
		CHASEDB1	0.9798	0.7530	0.9863
Yang et al. [220]	Grayscale conversion, Normalization, Gradient histogram equalization, Gamma correction	DRIVE	0.9579	0.8353	0.9751
		STARE	0.9626	0.7946	0.9821
		CHASEDB1	0.9632	0.8176	0.9776
Li et al. [221]	Green channel analysis, CLAHE	DRIVE	0.9769	0.8145	0.9883
		STARE	0.9797	0.8505	0.9889
		CHASEDB1	0.9803	0.9334	0.9862
Wu et al. [222]	Grayscale transform, Normalization	DRIVE	0.9686	0.8043	0.9844
		CHASEDB1	0.9746	0.8099	0.9856
Zhang et al. [223]	–	DRIVE	0.9701	0.7719	0.9799
		STARE	0.9691	0.6912	0.9911
		CHASEDB1	0.9811	0.8506	0.9981
Zhang et al. [224]	CLAHE, Gamma correction, Standardization	DRIVE	0.9565	0.7853	0.9812
		STARE	0.9668	0.8002	0.9864
		CHASEDB1	0.9667	0.8131	0.9840
Yang et al. [225]	CLAHE	DRIVE	0.9670	0.8133	0.9818
		STARE	0.9724	0.8201	0.9851
		CHASEDB1	0.9718	0.8209	0.9816
Dong et al. [226]	Grayscale transform, Normalization, CLAHE, Gamma correction	DRIVE	0.9586	0.7954	–
		CHASEDB1	0.9659	0.8259	

Table 10
Overview of approaches using GAN for retinal image segmentation.

Reference	Preprocessing	Database	Acc	Sn	Sp
Tu et al. [234]	–	DRIVE	9571	0.784	0.985
Gu et al. [235]	Data augmentation (flipping)	DRIVE	9545	0.8309	–
Wu et al. [236]	Data augmentation (translation, rotation, shearing and scaling)	DRIVE	9615	0.7798	0.982
Dong et al. [237]	Extraction of patches, Data augmentation (rotation, flipping, scaling)	DRIVE	0.9729	0.8579	0.9828
		STARE	0.9716	0.8126	0.9837
Park et al. [194]	Automatic color equalization	DRIVE	0.9706	0.8346	0.9836
		STARE	0.9876	0.8324	0.9938
		CHASEDB1	0.9736	0.8640	0.9745 -
		HRF	0.9761	0.9852	
Lahiri et al. [238]	Extraction of patches	DRIVE	0.950	–	–
		STARE	0.960		
Yang et al. [239]	Data augmentation (rotation, flipping), Z-score Normalization	DRIVE	0.9560	0.8340	0.9820
		STARE	0.9663	0.8334	0.9897
Guo et al. [16]	Data augmentation (rotation, translation, zooming, inversion and filling), Extraction of patches, Z-score Normalization	DRIVE	0.9542	0.8283	0.9726
Ma et al. [240]	Extraction of patches	DRIVE	0.913	0.794	0.982
		STARE	0.910	0.774	0.980
		XCAD	0.945	0.583	0.972
Zhou et al. [241]	–	DRIVE	0.9519	0.7412	0.9830
		STARE	0.9613	0.8334	0.9865
		CHASEDB1	0.9547	0.8134	0.9750
		HRF	0.9465	0.8003	0.9779
Zhao and Feng [242]	CLAHE, Gamma correction, Normalization	DRIVE	0.9565	0.8314	0.9757
		STARE	0.9690	0.8378	0.9838
Yang et al. [243],	Data augmentation called image stitching	DRIVE	0.9559	0.7659	0.9746
Kar et al. [244]	Grayscale transformation, Data augmentation (flipping), CLAHE, Z-score Normalization	DRIVE	0.9742	0.8936	0.9876
		STARE	0.9486	0.8441	0.9640
		CHASEDB1	0.9873	0.9335	0.9835
		HRF ARIA	0.9773	0.8885	0.9854
		IOSTAR	0.9628	0.7177	0.9840
		RC-SLO	0.9610	0.7807	0.9788
			0.9777	0.8714	0.9871
Alimanov and Islam [245]	Data augmentation (rotation, flipping)	DRIVE	0.9659	0.7829	–
		STARE	0.9697	0.8010	
		CHASEDB1	0.9665	0.8088	
Lin et al. [246]	Data augmentation (random cropping, random rotation, scaling, translation, flipping), Blur processing, Elastic deformation, CLAHE, random sharpening, random brightness contrast	DRIVE	0.9529	0.8626	0.9664
		STARE HRF	0.9679	0.8619	0.9807
			0.9629	0.8653	0.9729
Yue et al. [247]	Data augmentation (rotation, flipping), Grayscale transform, CLAHE	DRIVE	0.9567	0.8422	0.9825
		CHASEDB1	0.9671	0.8503	0.9850
Yue et al. [248]	Green channel analysis, CLAHE, Gamma correction, Data augmentation (rotation, mirroring, translation)	DRIVE	0.9702	0.8337	0.9850
		STARE	0.9712	0.8344	0.9884
		CHASEDB1	0.9673	0.8132	0.9837
Gu and Xu [249]	Extraction of patches, Data augmentation (rotation, color, saturation, brightness)	DRIVE	0.9571	0.8064	0.9790
		STARE	0.9786	0.7930	0.9910
		CHASEDB1	0.9756	0.8661	0.9836

SWD metric to measure the similarity between the generated image and the real image based on the detail feature.

Alimanov and Islam [245] addressed the problems of low-quality retinal image restoration and vessel segmentation. To do this, the authors proposed a retinal image restoration method based on a cycle-consistent generative adversarial network, Cycle-CBAM, that relies on unpaired low-quality and high-quality retrieved images before proposing the retinal vessel segmentation method CBAM-UNet. The authors reported accuracies of 0.9659, 0.9697, and 0.9665 on DRIVE, STARE, and CHASE_DB1 databases, respectively.

Yue et al. [247] proposed a method that uses GAN combined with SE-ResNet and dilated inception block for the segmenting retinal vessels, called SAD-GAN. The authors replaced the original convolution block with SE-ResNet module in the GAN generator. SE-Net is used to extract the global channel information, while concomitantly strengthening and weakening the key features and invalid features, respectively. The model was tested on DRIVE and CHASE_DB1 obtaining an accuracy of 0.9567 and 0.9671, respectively.

Yue et al. [248] proposed an improved GAN for retinal image segmentation based on R2U-Net. The authors applied in the generator an attention mechanism, channel, and spatial attention, to reduce the loss of information and extract more effective features. Furthermore, they used dense connection modules in the discriminator. The values of AUC were 0.9869, 0.9894, and 0.9885 on DRIVE, CHASE-DB1 and STARE, respectively.

Kar et al. [244] proposed a multi-scale residual convolutional neural network (MSR-Net), for retinal blood vessels segmentation, combined with GAN. The generator in the GAN architecture uses deep residual blocks with skip connections in UNet backbone. This model was tested on various publicly available databases (DRIVE, STARE, CHASE_DB1, HRF, ARIA, IOSTAR, and RC-SLO).

Gu and Xu [249] improved the retinal vessel segmentation through iterative refinement and reducing topological error. To do this, the authors proposed a GAN model to reduce topological discrepancies between the probability map of our segmentation results and the ground truth of real retinal vessels and introduced a recurrent neural network with the iterative prediction strategy that can improve the segmentation model to correct the prediction errors and tackle the problem of overfitting. The authors reported accuracies of 0.9571, 0.9786, and 0.9756 on DRIVE, STARE, and CHASE_DB1 databases, respectively.

In summary, deep learning is indeed an essential subarea of machine learning that has made significant advancements in image segmentation of retinal blood vessels. In this paper, we categorize several approaches for retinal vessel segmentation into four groups based on their network architecture: Convolutional Neural Network (CNN), Fully Convolutional Network (FCN), U-Net, and Generative Adversarial Network (GAN).

In CNN approaches, the blood vessels may be precisely identified by learning hierarchical characteristics from images. Authors have explored various customized and traditional CNN architectures. As described in Table 7, different authors reported accuracy for their models above 0.94. However, despite the great success of CNN in discovering strong spatially local correlations on databases of retinal blood images at various abstraction levels, one of the main issues with using a typical CNN for segmenting vessels is the requirement to divide a given image into a very large number of small patches and classify each of them, causing a high computational cost. To overcome the shortcomings of CNN approaches, the FNC technique is introduced. FCN is designed to work with input images of arbitrary sizes, making them more adaptable to different imaging conditions. However, FCN may face challenges in spatial loss of information (due to the downsampling and upsampling operations), but even so, the results are encouraging. Different authors reported accuracies around 0.96 (see Table 8). An especial and promising FCN architecture is U-Net, this architecture combines traditional convolutional layers with upsampling to learn both local and global features. Moreover, different authors have used different strategies to prevent spatial loss of information. The U-Net approaches have achieved up to 0.98 inaccuracies (see Table 9), but U-Net still struggles to precisely segment very thin blood vessels.

On the other hand, the limited size and diversity of annotated databases can hinder the performance of deep learning models, therefore, data availability remains a crucial challenge in retinal blood vessel segmentation. Many authors explored the potential of GAN as an automatic data augmentation technique, obtaining models with accuracies around 0.95. This is reported in Table 10. Finally, the trend toward using the U-Net architecture is likely to continue as it continues to show strong performance in retinal vessel segmentation and other medical image analysis tasks. However, It is important to note that deep learning methods for retinal vessel segmentation are continuously evolving, and authors are exploring a variety of strategies to achieve even better results.

7. Trends of retinal vessel segmentation

Currently, retinal vessel segmentation algorithms have become an essential component of automatic systems that are responsible for the detection of retinal diseases. This section mentions an analysis carried out taking into account research works that have already been published, in order to refer to the extent of the study related to the subject.

The search engines used to retrieve publications were IEEExplore, ScienceDirect and Springer, the search only included research articles published by journals related to the area of study such as artificial intelligence applied to medicine, expert systems and their applications, as well as neuroscience and computing., to mention a few areas. For this study, recent articles were considered, taking into account from 2015 to 2022. This allowed the analysis to be kept up to date.

Figs. 7–9 show the total distribution of articles published for each year depending on the search engine used, which are related to the segmentation of retinal vessels:

Traditional image segmentation techniques like thresholding, edge detection, and region-growing have been around for a while, and each has advantages and disadvantages. While they worked well in certain straightforward settings, they frequently had trouble with complex scenes, different lighting situations, and object occlusions, to name a few. However, image segmentation has made significant strides since deep learning emerged. By automatically learning relevant features directly from the raw data, deep learning-based techniques have revolutionized image segmentation and made it more precise and effective. This remarkable improvement is due, in part, to the following factors: Feature learning (the ability to learn and discover informative and relevant features from data), End to End learning (simultaneously training all parameters, i.e., learning every step from the beginning input stage to the final output outcome); Adaptability (aptitude for successfully adjusting to and acquiring knowledge from new information), among others.

8. Conclusions

This paper carried out a comprehensive review of recent approaches to machine learning methods for retinal blood vessel segmentation. The automation of medical image segmentation provides countless advantages to medical practitioners, reducing human error in determining existing conditions and prognoses and accelerating the application of medical treatment. In this survey, different retinal vessel segmentation approaches are studied to recollect the state-of-the-art in a single accessible manuscript. This manuscript can be used to guide the proper preprocessing and segmentation techniques based on the characteristics of specific retinal vessel segmentation real-world problems.

Nowadays, deep learning methods have been extensively used for image segmentation including retinal blood vessel images since they do not need any handcrafted features and outperform existing traditional machine learning methods. Despite the great success of deep learning, there are still some obstacles that require an in-depth examination and analysis in retinal blood vessel segmentation, such as the loss of microvasculature details at the end of vessels, preservation of capillaries, vascular structures of complex bifurcation, the false recognition of the lesion area, the fracture of the small vessel segmentation, a noisy environment (without any additional processing), the impact of loss function selection, among others.

The trend in blood vessel segmentation is to use and enhance previous deep-learning network architectures. This approach has shown significant impact and improvement in segmentation performance. We observed that many authors have built upon the foundations of encoder–decoder U-Net networks with short and long skip connections to enhance segmentation performance after evaluating various networks. Nevertheless, despite major advancements achieved with U-Net networks, blood vessel segmentation is still a difficult process, and there are still a number of issues that researchers deal with in this area.

1. The precise segmentation of very thin blood vessels remains a challenging task. Algorithms have trouble capturing the small features and identifying thin vessels apart from background pixels or noise.
2. A large volume of annotated data is necessary for the training models. However, it might be difficult to get large-scale annotated databases for blood vessel segmentation, particularly for uncommon or particular vascular diseases.
3. Models that perform well on one database may not generalize well to another due to the domain shift. This is because the degree of image quality, the appearance of the vessels, and the size of the vessels may differ amongst databases.

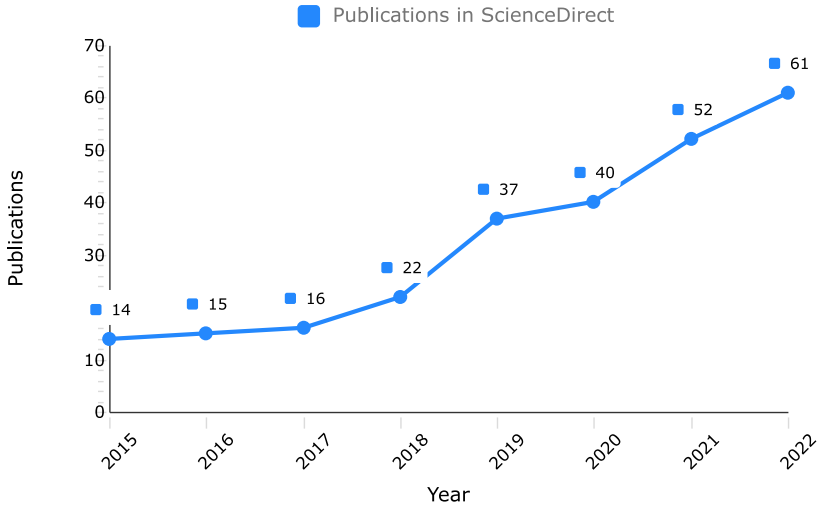

Fig. 7. Number of publications in ScienceDirect from 2015–2022.

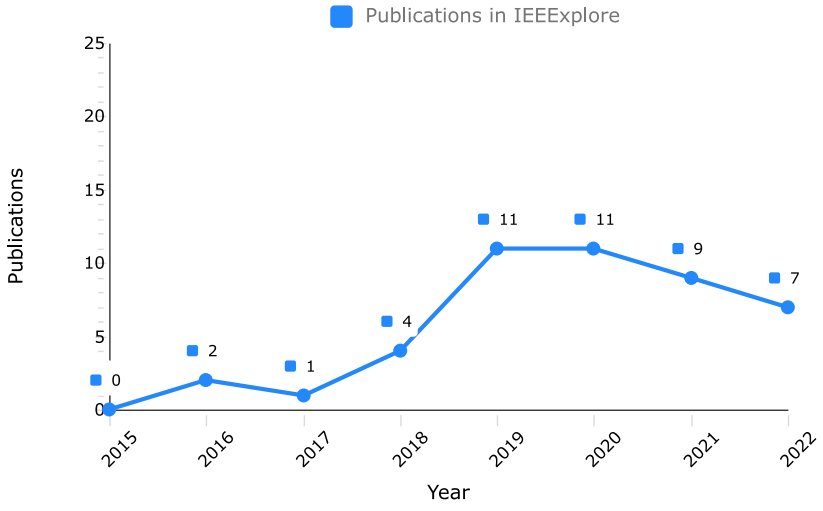

Fig. 8. Number of publications in IEEEXplore from 2015–2022.

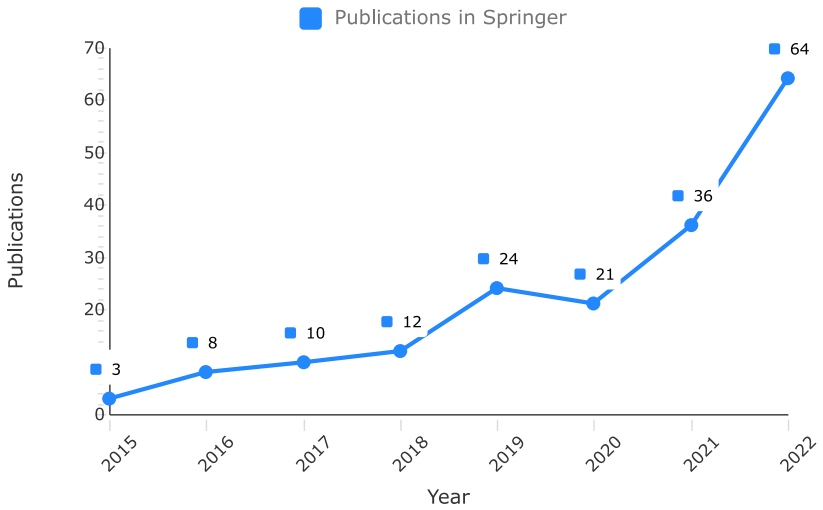

Fig. 9. Number of publications in Springer from 2015–2022.

Declaration of competing interest

The authors declare that they have no known competing financial interests or personal relationships that could have appeared to influence the work reported in this paper.

Acknowledgment

This work was supported by the research project grant: 6525/2022CIB, UAEMex.

References

[1] R. Benes, J. Karasek, R. Burget, K. Riha, Automatically designed machine vision system for the localization of CCA transverse section in ultrasound images, Comput. Methods Programs Biomed. 109 (1) (2013) 92–103.
[2] A. Garcia-Martinez, J.M. Vicente-Samper, J.M. Sabater-Navarro, Automatic detection of surgical haemorrhage using computer vision, Artif. Intell. Med. 78 (2017) 55–60.
[3] T. Khan, D. Nyholm, J. Westin, M. Dougherty, A computer vision framework for finger-tapping evaluation in parkinson's disease, Artif. Intell. Med. 60 (1) (2014) 27–40.
[4] M. Zortea, T.R. Schopf, K. Thon, M. Geilhufe, K. Hindberg, H. Kirchesch, K. Møllersen, J. Schulz, S.O. Skrøvseth, F. Godtliebsen, Performance of a dermoscopy-based computer vision system for the diagnosis of pigmented skin lesions compared with visual evaluation by experienced dermatologists, Artif. Intell. Med. 60 (1) (2014) 13–26.
[5] D.A. Wood, S. Kafiabadi, A.A. Busaidi, E. Guilhem, A. Montvila, J. Lynch, M. Townend, S. Agarwal, A. Mazumder, G.J. Barker, S. Ourselin, J.H. Cole, T.C. Booth, Deep learning models for triaging hospital head MRI examinations, Med. Image Anal. 78 (2022) 102391.
[6] T. Kaur, T.K. Gandhi, Automated brain image classification based on VGG-16 and transfer learning, in: 2019 International Conference on Information Technology, ICIT, IEEE, 2019.
[7] T. Kossen, P. Subramaniam, V.I. Madai, A. Hennemuth, K. Hildebrand, A. Hilbert, J. Sobesky, M. Livne, I. Galinovic, A.A. Khalil, J.B. Fiebach, D. Frey, Synthesizing anonymized and labeled TOF-MRA patches for brain vessel segmentation using generative adversarial networks, Comput. Biol. Med. 131 (2021) 104254.
[8] G. Urbanos, A. Martín, G. Vázquez, M. Villanueva, M. Villa, L. Jimenez-Roldan, M. Chavarrías, A. Lagares, E. Juárez, C. Sanz, Supervised machine learning methods and hyperspectral imaging techniques jointly applied for brain cancer classification, Sensors 21 (11) (2021) 3827.
[9] J.P. Appleton, L.J. Woodhouse, A. Adami, J.L. Becker, E. Berge, L.A. Cala, A.M. Casado, V. Caso, H.K. Christensen, R.A. Dineen, J. Gommans, P. Koumellis, S. Szatmari, N. Sprigg, P.M. Bath, J.M. Wardlaw, for the ENOS Investigators, Imaging markers of small vessel disease and brain frailty, and outcomes in acute stroke, Neurology 94 (5) (2020) e439–e452.
[10] O.A. Williams, E.A. Zeestraten, P. Benjamin, C. Lambert, A.J. Lawrence, A.D. Mackinnon, R.G. Morris, H.S. Markus, T.R. Barrick, R.A. Charlton, Predicting dementia in cerebral small vessel disease using an automatic diffusion tensor image segmentation technique, Stroke 50 (10) (2019) 2775–2782.
[11] C. Sperber, A. Hakim, L. Gallucci, D. Seiffge, B. Rezny-Kasprzak, E. Jäger, T. Meinel, R. Wiest, U. Fischer, M. Arnold, R. Umarova, A typology of cerebral small vessel disease based on imaging markers, J. Neurol. (2023).
[12] P. Deepa, M. Suganthi, A fuzzy shape representation of a segmented vessel tree and kernel-induced random forest classifier for the efficient prediction of lung cancer, J. Supercomput. 76 (8) (2019) 5801–5824.
[13] E.S.N. Joshua, M. Chakkravarthy, D. Bhattacharyya, An extensive review on lung cancer detection using machine learning techniques: A systematic study, Revue d'Intell. Artif. 34 (3) (2020) 351–359.
[14] J. Su, Z. Liu, J. Zhang, V.S. Sheng, Y. Song, Y. Zhu, Y. Liu, DV-net: Accurate liver vessel segmentation via dense connection model with D-BCE loss function, Knowl.-Based Syst. 232 (2021) 107471.
[15] M. Xu, Y. Wang, Y. Chi, X. Hua, Training liver vessel segmentation deep neural networks on noisy labels from contrast CT imaging, in: 2020 IEEE 17th International Symposium on Biomedical Imaging, ISBI, IEEE, 2020.
[16] X. Guo, C. Chen, Y. Lu, K. Meng, H. Chen, K. Zhou, Z. Wang, R. Xiao, Retinal vessel segmentation combined with generative adversarial networks and dense U-net, IEEE Access 8 (2020) 194551–194560.
[17] J. Poletti, M. Bach, S. Yang, R. Sexauer, B. Stieltjes, D.C. Rotzinger, J. Bremerich, A.W. Sauter, T. Weikert, Automated lung vessel segmentation reveals blood vessel volume redistribution in viral pneumonia, Eur. J. Radiol. 150 (2022) 110259.
[18] L. Zhou, X. Meng, Y. Huang, K. Kang, J. Zhou, Y. Chu, H. Li, D. Xie, J. Zhang, W. Yang, N. Bai, Y. Zhao, M. Zhao, G. Wang, L. Carin, X. Xiao, K. Yu, Z. Qiu, X. Gao, An interpretable deep learning workflow for discovering subvisual abnormalities in CT scans of COVID-19 inpatients and survivors, Nat. Mach. Intell. 4 (5) (2022) 494–503.
[19] H. Wen, J.A. Huapaya, S.M. Kanth, J. Sun, B.P. Matthew, S.C. Lee, M. Do, M.Y. Chen, A.A. Malayeri, A.F. Suffredini, Quantitative CT metrics associated with variability in the diffusion capacity of the lung of post-COVID-19 patients with minimal residual lung lesions, J. Imaging 9 (8) (2023) 150.
[20] J. Jacob, M. Pienn, C. Payer, M. Urschler, M. Kokosi, A. Devaraj, A.U. Wells, H. Olschewski, Quantitative CT-derived vessel metrics in idiopathic pulmonary fibrosis: A structure–function study, Respirology 24 (5) (2019) 445–452.
[21] H. Sun, X. Yang, X. Sun, X. Meng, H. Kang, R. Zhang, H. Zhang, M. Liu, H. Dai, C. Wang, Lung shrinking assessment on HRCT with elastic registration technique for monitoring idiopathic pulmonary fibrosis, Eur. Radiol. 33 (4) (2022) 2279–2288.
[22] Q. Yan, B. Wang, W. Zhang, C. Luo, W. Xu, Z. Xu, Y. Zhang, Q. Shi, L. Zhang, Z. You, Attention-guided deep neural network with multi-scale feature fusion for liver vessel segmentation, IEEE J. Biomed. Health Inform. 25 (7) (2021) 2629–2642.
[23] Y. Jin, A. Pepe, J. Li, C. Gsaxner, F.-h. Zhao, K.L. Pomykala, J. Kleesiek, A.F. Frangi, J. Egger, AI-based aortic vessel tree segmentation for cardiovascular diseases treatment: Status quo, 2021, http://dx.doi.org/10.48550/ARXIV.2108.02998.
[24] Z. Gao, L. Wang, R. Soroushmehr, A. Wood, J. Gryak, B. Nallamothu, K. Najarian, Vessel segmentation for X-ray coronary angiography using ensemble methods with deep learning and filter-based features, BMC Med. Imaging 22 (1) (2022).
[25] Z. Jiang, C. Ou, Y. Qian, R. Rehan, A. Yong, Coronary vessel segmentation using multiresolution and multiscale deep learning, Inform. Med. Unlocked 24 (2021) 100602.
[26] Z. Xian, X. Wang, S. Yan, D. Yang, J. Chen, C. Peng, Main coronary vessel segmentation using deep learning in smart medical, in: C. Huang (Ed.), Math. Probl. Eng. 2020 (2020) 1–9.
[27] R. Zhou, F. Guo, M.R. Azarpazhooh, J.D. Spence, E. Ukwatta, M. Ding, A. Fenster, A voxel-based fully convolution network and continuous max-flow for carotid vessel-wall-volume segmentation from 3D ultrasound images, IEEE Trans. Med. Imaging 39 (9) (2020) 2844–2855.
[28] C. Wu, Y. Zou, Z. Yang, U-GAN: Generative adversarial networks with U-net for retinal vessel segmentation, in: 2019 14th International Conference on Computer Science & Education, (ICCSE), 2019, pp. 642–646.
[29] H. Wu, W. Wang, J. Zhong, B. Lei, Z. Wen, J. Qin, SCS-net: A scale and context sensitive network for retinal vessel segmentation, Med. Image Anal. 70 (2021) 102025.
[30] C. Guo, M. Szemenyei, Y. Yi, W. Wang, B. Chen, C. Fan, SA-UNet: Spatial attention U-net for retinal vessel segmentation, in: 2020 25th International Conference on Pattern Recognition, ICPR, IEEE, 2021.
[31] X. Tang, B. Zhong, J. Peng, B. Hao, J. Li, Multi-scale channel importance sorting and spatial attention mechanism for retinal vessels segmentation, Appl. Soft Comput. 93 (2020) 106353.
[32] M. Abràmoff, C.N. Kay, Image processing, in: Retina, Elsevier, 2013, pp. 151–176.
[33] R.J. Chalakkal, W.H. Abdulla, S.C. Hong, Fundus retinal image analyses for screening and diagnosing diabetic retinopathy, macular edema, and glaucoma disorders, in: Diabetes and Fundus OCT, Elsevier, 2020, pp. 59–111.
[34] M.R.K. Mookiah, S. Hogg, T.J. MacGillivray, V. Prathiba, R. Pradeepa, V. Mohan, R.M. Anjana, A.S. Doney, C.N. Palmer, E. Trucco, A review of machine learning methods for retinal blood vessel segmentation and artery/vein classification, Med. Image Anal. 68 (2021) 101905.
[35] M. Fraz, P. Remagnino, A. Hoppe, B. Uyyanonvara, A. Rudnicka, C. Owen, S. Barman, Blood vessel segmentation methodologies in retinal images – a survey, Comput. Methods Programs Biomed. 108 (1) (2012) 407–433.
[36] C.L. Srinidhi, P. Aparna, J. Rajan, Automated method for retinal artery/vein separation via graph search metaheuristic approach, IEEE Trans. Image Process. 28 (6) (2019) 2705–2718.
[37] J. Staal, M. Abramoff, M. Niemeijer, M. Viergever, B. van Ginneken, Ridge based vessel segmentation in color images of the retina, IEEE Trans. Med. Imaging 23 (4) (2004) 501–509.
[38] A. Hoover, V. Kouznetsova, M. Goldbaum, Locating blood vessels in retinal images by piecewise threshold probing of a matched filter response, IEEE Trans. Med. Imaging 19 (3) (2000) 203–210.
[39] D. Farnell, F. Hatfield, P. Knox, M. Reakes, S. Spencer, D. Parry, S. Harding, Enhancement of blood vessels in digital fundus photographs via the application of multiscale line operators, J. Franklin Inst. B 345 (7) (2008) 748–765.
[40] T. Kauppi, V. Kalesnykiene, J. Kämäräinen, L. Lensu, I. Sorri, A. Raninen, R. Voutilainen, H. Uusitalo, H. Kälviäinen, J. Pietilä, The DIARETDB1 diabetic retinopathy database and evaluation protocol, in: BMVC, 2007.
[41] E. Decencière, X. Zhang, G. Cazuguel, B. Lay, B. Cochener, C. Trone, P. Gain, R. Ordonez, P. Massin, A. Erginay, B. Charton, J.-C. Klein, Feedback on a publicly distributed image database: The messidor database, Image Anal. Stereol. 33 (3) (2014) 231.
[42] M.M. Fraz, P. Remagnino, A. Hoppe, B. Uyyanonvara, A.R. Rudnicka, C.G. Owen, S.A. Barman, An ensemble classification-based approach applied to retinal blood vessel segmentation, IEEE Trans. Biomed. Eng. 59 (9) (2012) 2538–2548.

[43] M. Niemeijer, B. van Ginneken, M.J. Cree, A. Mizutani, G. Quellec, C.I. Sanchez, B. Zhang, R. Hornero, M. Lamard, C. Muramatsu, X. Wu, G. Cazuguel, J. You, A. Mayo, Q. Li, Y. Hatanaka, B. Cochener, C. Roux, F. Karray, M. Garcia, H. Fujita, M.D. Abramoff, Retinopathy online challenge: Automatic detection of microaneurysms in digital color fundus photographs, IEEE Trans. Med. Imaging 29 (1) (2010) 185–195.

[44] B. Al-Diri, A. Hunter, D. Steel, M. Habib, T. Hudaib, S. Berry, REVIEW - A reference data set for retinal vessel profiles, in: 2008 30th Annual International Conference of the IEEE Engineering in Medicine and Biology Society, IEEE, 2008.

[45] R.G. Aastha, A review on retinal blood vessel segmentation methodologies, Int. J. Sci. Technol. Res. 8 (9) (2019).

[46] S. Chaudhuri, S. Chatterjee, N. Katz, M. Nelson, M. Goldbaum, Detection of blood vessels in retinal images using two-dimensional matched filters, IEEE Trans. Med. Imaging 8 (3) (1989) 263–269.

[47] D. Marín, A. Aquino, M.E. Gegúndez-Arias, J.M. Bravo, A new supervised method for blood vessel segmentation in retinal images by using gray-level and moment invariants-based features, IEEE Trans. Med. Imaging 30 (1) (2010) 146–158.

[48] N. Singh, L. Kaur, A survey on blood vessel segmentation methods in retinal images, in: 2015 International Conference on Electronic Design, Computer Networks & Automated Verification, (EDCAV), IEEE, 2015, pp. 23–28.

[49] S. Moccia, E.D. Momi, S.E. Hadji, L.S. Mattos, Blood vessel segmentation algorithms — Review of methods, datasets and evaluation metrics, Comput. Methods Programs Biomed. 158 (2018) 71–91.

[50] M.M. Fraz, P. Remagnino, A. Hoppe, B. Uyyanonvara, A.R. Rudnicka, C.G. Owen, S.A. Barman, Blood vessel segmentation methodologies in retinal images–A survey, Comput. Methods Programs Biomed. 108 (1) (2012) 407–433.

[51] S. Biradar, A. Jadhav, A survey on blood vessel segmentation and optic disc segmentation of retinal images, Int. J. Adv. Res. Comput. Commun. Eng. 4 (5) (2015) 21–26.

[52] N. Eling, N. Damond, T. Hoch, B. Bodenmiller, Cytomapper : An R/Bioconductor package for visualization of highly multiplexed imaging data, in: Z. Lu (Ed.), Bioinformatics 36 (24) (2020) 5706–5708.

[53] L. Shang, D.-S. Huang, J.-X. Du, C.-H. Zheng, Palmprint recognition using FastICA algorithm and radial basis probabilistic neural network, Neurocomputing 69 (13–15) (2006) 1782–1786.

[54] K.-H. Liu, D.-S. Huang, Cancer classification using rotation forest, Comput. Biol. Med. 38 (5) (2008) 601–610.

[55] Z.-Q. Zhao, D.-S. Huang, W. Jia, Palmprint recognition with 2DPCA+pca based on modular neural networks, Neurocomputing 71 (1–3) (2007) 448–454.

[56] J.-X. Du, D.-S. Huang, X.-F. Wang, X. Gu, Computer-aided plant species identification (CAPSI) based on leaf shape matching technique, Trans. Inst. Meas. Control 28 (3) (2006) 275–285.

[57] X.-F. Wang, D.-S. Huang, J.-X. Du, H. Xu, L. Heutte, Classification of plant leaf images with complicated background, Appl. Math. Comput. 205 (2) (2008) 916–926.

[58] J.-X. Mi, D.-S. Huang, B. Wang, X. Zhu, The nearest-farthest subspace classification for face recognition, Neurocomputing 113 (2013) 241–250.

[59] B. Li, C.-H. Zheng, D.-S. Huang, Locally linear discriminant embedding: An efficient method for face recognition, Pattern Recognit. 41 (12) (2008) 3813–3821.

[60] S. Rani, S. Jindal, B. Kaur, A brief review on image restoration techniques, Int. J. Comput. Appl. 150 (12) (2016) 30–33.

[61] Y. Zhao, D.-S. Huang, W. Jia, Completed local binary count for rotation invariant texture classification, IEEE Trans. Image Process. 21 (10) (2012) 4492–4497.

[62] Z.-L. Sun, D.-S. Huang, Y.-M. Cheun, Extracting nonlinear features for multispectral images by FCMC and KPCA, Digit. Signal Process. 15 (4) (2005) 331–346.

[63] Z.-Q. Zhao, H. Glotin, Z. Xie, J. Gao, X. Wu, Cooperative sparse representation in two opposite directions for semi-supervised image annotation, IEEE Trans. Image Process. 21 (9) (2012) 4218–4231.

[64] Z.-L. Sun, D.-S. Huang, Y.-M. Cheung, J. Liu, G.-B. Huang, Using FCMC, FVS, and PCA techniques for feature extraction of multispectral images, IEEE Geosci. Remote Sens. Lett. 2 (2) (2005) 108–112.

[65] J.-H. Han, D.-S. Huang, T.-M. Lok, M. Lyu, A novel image retrieval system based on BP neural network, in: Proceedings. 2005 IEEE International Joint Conference on Neural Networks, 2005., IEEE, 2005.

[66] J.-H. Han, D.-S. Huang, A novel BP-based image retrieval system, in: 2005 IEEE International Symposium on Circuits and Systems, IEEE, 2005.

[67] X.-F. Wang, D.-S. Huang, H. Xu, An efficient local Chan–Vese model for image segmentation, Pattern Recognit. 43 (3) (2010) 603–618.

[68] X. Wang, D. shuang Huang, A novel multi-layer level set method for image segmentation, J. Univers. Comput. Sci. 14 (2008) 2427–2452.

[69] B. Li, C. Wang, D.-S. Huang, Supervised feature extraction based on orthogonal discriminant projection, Neurocomputing 73 (1–3) (2009) 191–196.

[70] B. Li, D.-S. Huang, C. Wang, K.-H. Liu, Feature extraction using constrained maximum variance mapping, Pattern Recognit. 41 (11) (2008) 3287–3294.

[71] C.-Y. Lu, D.-S. Huang, Optimized projections for sparse representation based classification, Neurocomputing 113 (2013) 213–219.

[72] F. Garcia-Lamont, J. Cervantes, A. López, L. Rodriguez, Segmentation of images by color features: A survey, Neurocomputing 292 (2018) 1–27.

[73] K. Fu, J. Mui, A survey on image segmentation, Pattern Recognit. 13 (1) (1981) 3–16.

[74] T.R. Singh, S. Roy, O.I. Singh, T. Sinam, K.M. Singh, A new local adaptive thresholding technique in binarization, ArXiv (2012) arXiv:1201.5227.

[75] M. Sonka, V. Hlavac, R. Boyle, Image Processing, Analysis, and Machine Vision, Thomson-Engineering, 2007.

[76] M. Alhussein, K. Aurangzeb, S.I. Haider, An unsupervised retinal vessel segmentation using hessian and intensity based approach, IEEE Access 8 (2020) 165056–165070.

[77] K. Bahadar Khan, A. A. Khaliq, M. Shahid, A morphological hessian based approach for retinal blood vessels segmentation and denoising using region based otsu thresholding, PLoS One 11 (7) (2016) e0158996.

[78] Z. Jiang, J. Yepez, S. An, S. Ko, Fast, accurate and robust retinal vessel segmentation system, Biocybern. Biomed. Eng. 37 (3) (2017) 412–421.

[79] H. Wang, Y. Jiang, X. Jiang, J. Wu, X. Yang, Automatic vessel segmentation on fundus images using vessel filtering and fuzzy entropy, Soft Comput. 22 (5) (2018) 1501–1509.

[80] S. Mahapatra, U. Jena, S. Dash, Mean global based on hysteresis thresholding for retinal blood vessel segmentation using enhanced homomorphic filtering, Multimedia Tools Appl. (2022) 1–18.

[81] C. Yao, H.-j. Chen, Automated retinal blood vessels segmentation based on simplified PCNN and fast 2D-Otsu algorithm, J. Central South Univ. Technol. 16 (4) (2009) 640–646.

[82] O. Ali, N. Muhammad, Z. Jadoon, B.M. Kazmi, N. Muzamil, Z. Mahmood, A comparative study of automatic vessel segmentation algorithms, in: 2020 3rd International Conference on Computing, Mathematics and Engineering Technologies, (ICoMET), IEEE, 2020, pp. 1–6.

[83] H. Aguirre-Ramos, J.G. Avina-Cervantes, I. Cruz-Aceves, J. Ruiz-Pinales, S. Ledesma, Blood vessel segmentation in retinal fundus images using gabor filters, fractional derivatives, and expectation maximization, Appl. Math. Comput. 339 (2018) 568–587.

[84] U. Ozkava, S. Ozturk, B. Akdemir, L. Sevfi, An efficient retinal blood vessel segmentation using morphological operations, in: 2018 2nd International Symposium on Multidisciplinary Studies and Innovative Technologies, (ISMSIT), IEEE, 2018, pp. 1–7.

[85] J. Dash, N. Bhoi, A thresholding based technique to extract retinal blood vessels from fundus images, Future Comput. Inform. J. 2 (2) (2017) 103–109.

[86] T. Mapayi, P.A. Owolawi, Automatic retinal vascular network detection using multi-thresholding approach based on otsu, in: 2019 International Multidisciplinary Information Technology and Engineering Conference, (IMITEC), IEEE, 2019, pp. 1–5.

[87] Y. Yin, M. Adel, S. Bourennane, Retinal vessel segmentation using a probabilistic tracking method, Pattern Recognit. 45 (4) (2012) 1235–1244.

[88] E. Moghimirad, S.H. Rezatofighi, H. Soltanian-Zadeh, Retinal vessel segmentation using a multi-scale medialness function, Comput. Biol. Med. 42 (1) (2012) 50–60.

[89] M.U. Akram, S.A. Khan, Multilayered thresholding-based blood vessel segmentation for screening of diabetic retinopathy, Eng. Comput. 29 (2) (2013) 165–173.

[90] D. Kaba, A.G. Salazar-Gonzalez, Y. Li, X. Liu, A. Serag, Segmentation of retinal blood vessels using gaussian mixture models and expectation maximisation, in: International Conference on Health Information Science, Springer, 2013, pp. 105–112.

[91] T. Chakraborti, D.K. Jha, A.S. Chowdhury, X. Jiang, A self-adaptive matched filter for retinal blood vessel detection, Mach. Vis. Appl. 26 (1) (2015) 55–68.

[92] J. Zhang, E. Bekkers, S. Abbasi, B. Dashtbozorg, B.t. Haar Romeny, Robust and fast vessel segmentation via Gaussian derivatives in orientation scores, in: International Conference on Image Analysis and Processing, Springer, 2015, pp. 537–547.

[93] N.P. Singh, R. Srivastava, Retinal blood vessels segmentation by using gumbel probability distribution function based matched filter, Comput. Methods Programs Biomed. 129 (2016) 40–50.

[94] Y. Yin, M. Adel, S. Bourennane, Automatic segmentation and measurement of vasculature in retinal fundus images using probabilistic formulation, Comput. Math. Methods Med. 2013 (2013).

[95] J. De, H. Li, L. Cheng, Tracing retinal vessel trees by transductive inference, BMC Bioinform. 15 (1) (2014) 1–20.

[96] D. Chen, L.D. Cohen, Piecewise geodesics for vessel centerline extraction and boundary delineation with application to retina segmentation, in: International Conference on Scale Space and Variational Methods in Computer Vision, Springer, 2015, pp. 270–281.

[97] S. Dash, S. Verma, M.S. Khan, M. Wozniak, J. Shafi, M.F. Ijaz, A hybrid method to enhance thick and thin vessels for blood vessel segmentation, Diagnostics 11 (11) (2021) 2017.

[98] J. De, L. Cheng, X. Zhang, F. Lin, H. Li, K.H. Ong, W. Yu, Y. Yu, S. Ahmed, A graph-theoretical approach for tracing filamentary structures in neuronal and retinal images, IEEE Trans. Med. Imaging 35 (1) (2015) 257–272.

[99] N. Tamim, M. Elshrkawey, G. Abdel Azim, H. Nassar, Retinal blood vessel segmentation using hybrid features and multi-layer perceptron neural networks, Symmetry 12 (6) (2020) 894.

[100] S.S.A. Hassan, D.B. Bong, M. Premsenthil, Detection of neovascularization in diabetic retinopathy, J. Digital Imaging 25 (3) (2012) 437–444.

[101] X. You, Q. Peng, Y. Yuan, Y.-m. Cheung, J. Lei, Segmentation of retinal blood vessels using the radial projection and semi-supervised approach, Pattern Recognit. 44 (10–11) (2011) 2314–2324.

[102] Y. Yin, M. Adel, M. Guillaume, S. Bourennane, A probabilistic based method for tracking vessels in retinal images, in: 2010 IEEE International Conference on Image Processing, IEEE, 2010, pp. 4081–4084.

[103] H. Li, J. Zhang, Q. Nie, L. Cheng, A retinal vessel tracking method based on bayesian theory, in: 2013 IEEE 8th Conference on Industrial Electronics and Applications, (ICIEA), IEEE, 2013, pp. 232–235.

[104] M. Adel, M. Rasigni, T. Gaidon, C. Fossati, S. Bourennane, Statistical-based linear vessel structure detection in medical images, in: 2009 16th IEEE International Conference on Image Processing, (ICIP), IEEE, 2009, pp. 649–652.

[105] K.K. Delibasis, A.I. Kechriniotis, C. Tsonos, N. Assimakis, Automatic model-based tracing algorithm for vessel segmentation and diameter estimation, Comput. Methods Programs Biomed. 100 (2) (2010) 108–122.

[106] Y.Q. Zhao, X.H. Wang, X.F. Wang, F.Y. Shih, Retinal vessels segmentation based on level set and region growing, Pattern Recognit. 47 (7) (2014) 2437–2446.

[107] R. Panda, N. Puhan, G. Panda, New binary hausdorff symmetry measure based seeded region growing for retinal vessel segmentation, Biocybern. Biomed. Eng. 36 (1) (2016) 119–129.

[108] B. Lam, H. Yan, A novel vessel segmentation algorithm for pathological retina images based on the divergence of vector fields, IEEE Trans. Med. Imaging 27 (2) (2008) 237–246.

[109] S. Jiménez, P. Alemany, I. Fondón, A. Foncubierta, B. Acha, C. Serrano, Automatic detection of vessels in color fundus images, Arch. Sociedad Española de Oftalmología (English Edition) 85 (3) (2010) 103–109.

[110] I. Lázár, A. Hajdu, Segmentation of retinal vessels by means of directional response vector similarity and region growing, Comput. Biol. Med. 66 (2015) 209–221.

[111] E.O. Rodrigues, A. Conci, P. Liatsis, ELEMENT: Multi-modal retinal vessel segmentation based on a coupled region growing and machine learning approach, IEEE J. Biomed. Health Inform. 24 (12) (2020) 3507–3519.

[112] C.I.O. Martins, F.N.S. Medeiros, R.M.S. Veras, F.N. Bezerra, R.M. Cesar, Evaluation of retinal vessel segmentation methods for microaneurysms detection, in: 2009 16th IEEE International Conference on Image Processing, ICIP, IEEE, 2009.

[113] R. Panda, N.B. Puhan, G. Panda, Hausdorff symmetry operator towards retinal blood vessel segmentation, in: 2014 19th International Conference on Digital Signal Processing, IEEE, 2014.

[114] B. Yin, H. Li, B. Sheng, X. Hou, Y. Chen, W. Wu, P. Li, R. Shen, Y. Bao, W. Jia, Vessel extraction from non-fluorescein fundus images using orientation-aware detector, Med. Image Anal. 26 (1) (2015) 232–242.

[115] L. Zhang, M. Fisher, W. Wang, Retinal vessel segmentation using multi-scale textons derived from keypoints, Comput. Med. Imaging Graph. 45 (2015) 47–56.

[116] R. GeethaRamani, L. Balasubramanian, Retinal blood vessel segmentation employing image processing and data mining techniques for computerized retinal image analysis, Biocybern. Biomed. Eng. 36 (1) (2016) 102–118.

[117] M.A. Khan, N. Mir, A. Sarirete, J.N. Carmichael, Thin vessel detection and thick vessel edge enhancement to boost performance of retinal vessel extraction methods, Procedia Comput. Sci. 163 (2019) 618–638.

[118] A.K. Shukla, R.K. Pandey, R.B. Pachori, A fractional filter based efficient algorithm for retinal blood vessel segmentation, Biomed. Signal Process. Control 59 (2020) 101883.

[119] C.-C. Chang, C.-C. Lin, P.-Y. Pai, Y.-C. Chen, A novel retinal blood vessel segmentation method based on line operator and edge detector, in: 2009 Fifth International Conference on Intelligent Information Hiding and Multimedia Signal Processing, IEEE, 2009, pp. 299–302.

[120] F. Orujov, R. Maskeliūnas, R. Damaševičius, W. Wei, Fuzzy based image edge detection algorithm for blood vessel detection in retinal images, Appl. Soft Comput. 94 (2020) 106452.

[121] B. Toptaş, D. Hanbay, Retinal blood vessel segmentation using pixel-based feature vector, Biomed. Signal Process. Control 70 (2021) 103053.

[122] J. Yang, M. Huang, J. Fu, C. Lou, C. Feng, Frangi based multi-scale level sets for retinal vascular segmentation, Comput. Methods Programs Biomed. 197 (2020) 105752.

[123] B.S. Tchinda, D. Tchiotsop, M. Noubom, V. Louis-Dorr, D. Wolf, Retinal blood vessels segmentation using classical edge detection filters and the neural network, Inform. Med. Unlocked 23 (2021) 100521.

[124] E.M. Sigurðsson, S. Valero, J.A. Benediktsson, J. Chanussot, H. Talbot, E. Stefánsson, Automatic retinal vessel extraction based on directional mathematical morphology and fuzzy classification, Pattern Recognit. Lett. 47 (2014) 164–171.

[125] X.-F. Wang, D.-S. Huang, A novel density-based clustering framework by using level set method, IEEE Trans. Knowl. Data Eng. 21 (11) (2009) 1515–1531.

[126] J.D. Gibson, A. Bovik (Eds.), Handbook of Image and Video Processing, first ed., Academic Press Inc., Orlando, FL, USA, 2000.

[127] J.C. Bezdek, R. Ehrlich, W. Full, FCM: The fuzzy c-means clustering algorithm, Comput. Geosci. 10 (2) (1984) 191–203.

[128] V.M. Saffarzadeh, A. Osareh, B. Shadgar, Vessel segmentation in retinal images using multi-scale line operator and K-means clustering, J. Med. Signals Sens. 4 (2014) 122–129.

[129] S.S. Mondal, N. Mandal, A. Singh, K.K. Singh, Blood vessel detection from retinal fundas images using GIFKCN classifier, Procedia Comput. Sci. 167 (2020) 2060–2069.

[130] M. Hashemzadeh, B.A. Azar, Retinal blood vessel extraction employing effective image features and combination of supervised and unsupervised machine learning methods, Artif. Intell. Med. 95 (2019) 1–15.

[131] A.E. Hassanien, E. Emary, H.M. Zawbaa, Retinal blood vessel localization approach based on bee colony swarm optimization, fuzzy c-means and pattern search, J. Vis. Commun. Image Represent. 31 (2015) 186–196.

[132] S.S. Kar, S.P. Maity, Blood vessel extraction and optic disc removal using curvelet transform and kernel fuzzy c-means, Comput. Biol. Med. 70 (2016) 174–189.

[133] G. Sun, X. Liu, S. Wang, L. Gao, M. Liu, Width measurement for pathological vessels in retinal images using centerline correction and k-means clustering, Measurement 139 (2019) 185–195.

[134] N. Memari, A.R. Ramli, M.I.B. Saripan, S. Mashohor, M. Moghbel, Retinal blood vessel segmentation by using matched filtering and fuzzy C-means clustering with integrated level set method for diabetic retinopathy assessment, J. Med. Biol. Eng. 39 (5) (2018) 713–731.

[135] K. Mardani, K. Maghooli, Enhancing retinal blood vessel segmentation in medical images using combined segmentation modes extracted by DBSCAN and morphological reconstruction, Biomed. Signal Process. Control 69 (2021) 102837.

[136] J.-X. Du, D.-S. Huang, X.-F. Wang, X. Gu, Shape recognition based on neural networks trained by differential evolution algorithm, Neurocomputing 70 (4–6) (2007) 896–903.

[137] D.-S. Huang, The Study of Data Mining Methods for Gene Expression Profiles, Science Press of China, China, 2009.

[138] W.-B. Zhao, D.-S. Huang, J.-Y. Du, L.-M. Wang, Genetic optimization of radial basis probabilistic neural networks, Int. J. Pattern Recognit. Artif. Intell. 18 (08) (2004) 1473–1499.

[139] F. Han, Q.-H. Ling, D.-S. Huang, An improved approximation approach incorporating particle swarm optimization and a priori information into neural networks, Neural Comput. Appl. 19 (2) (2009) 255–261.

[140] F. Han, D.-S. Huang, A new constrained learning algorithm for function approximation by encoding a priori information into feedforward neural networks, Neural Comput. Appl. 17 (5–6) (2007) 433–439.

[141] F. Han, D.-S. Huang, Improved extreme learning machine for function approximation by encoding a priori information, Neurocomputing 69 (16–18) (2006) 2369–2373.

[142] D.-S. Huang, J.-X. Du, A constructive hybrid structure optimization methodology for radial basis probabilistic neural networks, IEEE Trans. Neural Netw. 19 (12) (2008) 2099–2115.

[143] D.-S. Huang, A constructive approach for finding arbitrary roots of polynomials by neural networks, IEEE Trans. Neural Netw. 15 (2) (2004) 477–491.

[144] D.-S. Huang, Systematic Theory of Neural Networks for Pattern Recognition, Publishing House of Electronic Industry of China, China, 1996.

[145] D.-S. Huang, Radial basis probabilistic neural networks: Model and application, Int. J. Pattern Recognit. Artif. Intell. 13 (07) (1999) 1083–1101.

[146] D.-S. Huang, S.-D. Ma, Linear and nonlinear feedforward neural network classifiers: A comprehensive understanding, J. Intell. Syst. 9 (1) (1999) 1–38.

[147] C. Chen, J.H. Chuah, R. Ali, Y. Wang, Retinal vessel segmentation using deep learning: A review, IEEE Access 9 (2021) 111985–112004.

[148] T.A. Soomro, A.J. Afifi, L. Zheng, S. Soomro, J. Gao, O. Hellwich, M. Paul, Deep learning models for retinal blood vessels segmentation: A review, IEEE Access 7 (2019) 71696–71717.

[149] O.O. Sule, A survey of deep learning for retinal blood vessel segmentation methods: Taxonomy, trends, challenges and future directions, IEEE Access 10 (2022) 38202–38236.

[150] P.M. Samuel, T. Veeramalai, Multilevel and multiscale deep neural network for retinal blood vessel segmentation, Symmetry 11 (7) (2019).

[151] S. Wang, Y. Yin, G. Cao, B. Wei, Y. Zheng, G. Yang, Hierarchical retinal blood vessel segmentation based on feature and ensemble learning, Neurocomputing 149 (2015) 708–717.

[152] D. Maji, A. Santara, P. Mitra, D. Sheet, Ensemble of deep convolutional neural networks for learning to detect retinal vessels in fundus images, CoRR (2016) arXiv:1603.04833.

[153] P. Liskowski, K. Krawiec, Segmenting retinal blood vessels with deep neural networks, IEEE Trans. Med. Imaging 35 (11) (2016) 2369–2380.

[154] K.-K. Maninis, J. Pont-Tuset, P. Arbeláez, L. Van Gool, Deep retinal image understanding, in: S. Ourselin, L. Joskowicz, M.R. Sabuncu, G. Unal, W. Wells (Eds.), Medical Image Computing and Computer-Assisted Intervention – MICCAI 2016, Springer International Publishing, Cham, 2016, pp. 140–148.

[155] H. Fu, Y. Xu, D.W.K. Wong, J. Liu, Retinal vessel segmentation via deep learning network and fully-connected conditional random fields, in: 2016 IEEE 13th International Symposium on Biomedical Imaging, (ISBI), 2016, pp. 698–701.

[156] A. Wu, Z. Xu, M. Gao, M. Buty, D.J. Mollura, Deep vessel tracking: A generalized probabilistic approach via deep learning, in: 2016 IEEE 13th International Symposium on Biomedical Imaging, (ISBI), 2016, pp. 1363–1367.

[157] A.F. Khalaf, I.A. Yassine, A.S. Fahmy, Convolutional neural networks for deep feature learning in retinal vessel segmentation, in: 2016 IEEE International Conference on Image Processing, (ICIP), 2016, pp. 385–388.

[158] Z. Yao, Z. Zhang, L.-Q. Xu, Convolutional neural network for retinal blood vessel segmentation, in: 2016 9th International Symposium on Computational Intelligence and Design (ISCID), Vol. 1, 2016, pp. 406–409.

[159] H. Fu, Y. Xu, S. Lin, D.W. Kee Wong, J. Liu, DeepVessel: Retinal vessel segmentation via deep learning and conditional random field, in: S. Ourselin, L. Joskowicz, M.R. Sabuncu, G. Unal, W. Wells (Eds.), Medical Image Computing and Computer-Assisted Intervention – MICCAI 2016, Springer International Publishing, Cham, 2016, pp. 132–139.

[160] J.H. Tan, U.R. Acharya, S.V. Bhandary, K.C. Chua, S. Sivaprasad, Segmentation of optic disc, fovea and retinal vasculature using a single convolutional neural network, J. Comput. Sci. 20 (2017) 70–79.

[161] G. Tetteh, M. Rempfler, C. Zimmer, B.H. Menze, Deep-fext: Deep feature extraction for vessel segmentation and centerline prediction, in: Q. Wang, Y. Shi, H.-I. Suk, K. Suzuki (Eds.), Machine Learning in Medical Imaging, Springer International Publishing, Cham, 2017, pp. 344–352.

[162] Z. Feng, J. Yang, L. Yao, Patch-based fully convolutional neural network with skip connections for retinal blood vessel segmentation, in: 2017 IEEE International Conference on Image Processing, (ICIP), 2017, pp. 1742–1746.

[163] T.A. Soomro, A.J. Afifi, J. Gao, O. Hellwich, M.A.U. Khan, M. Paul, L. Zheng, Boosting sensitivity of a retinal vessel segmentation algorithm with convolutional neural network, in: 2017 International Conference on Digital Image Computing: Techniques and Applications, (DICTA), 2017, pp. 1–8.

[164] L. Ngo, J.-H. Han, Multi-level deep neural network for efficient segmentation of blood vessels in fundus images, Electron. Lett. 53 (16) (2017) 1096–1098.

[165] Y. Guo, Ü. Budak, L.J. Vespa, E. Khorasani, A. Şengür, A retinal vessel detection approach using convolution neural network with reinforcement sample learning strategy, Measurement 125 (2018) 586–591.

[166] Y. Jiang, N. Tan, T. Peng, H. Zhang, Retinal vessels segmentation based on dilated multi-scale convolutional neural network, IEEE Access 7 (2019) 76342–76352.

[167] D. Yang, M. Ren, B. Xu, Retinal blood vessel segmentation with improved convolutional neural networks, J. Med. Imag. Health Inform. 9 (2019) 1112–1118.

[168] C.-H. Hua, T. Huynh-The, S. Lee, Retinal vessel segmentation using round-wise features aggregation on bracket-shaped convolutional neural networks, in: 2019 41st Annual International Conference of the IEEE Engineering in Medicine and Biology Society, (EMBC), 2019, pp. 36–39.

[169] K.J. Noh, S.J. Park, S. Lee, Scale-space approximated convolutional neural networks for retinal vessel segmentation, Comput. Methods Programs Biomed. 178 (2019) 237–246.

[170] L. Yu, Z. Qin, T. Zhuang, Y. Ding, Z. Qin, K.-K. Raymond Choo, A framework for hierarchical division of retinal vascular networks, Neurocomputing 392 (2020) 221–232.

[171] E. Uysal, G.E. Güraksin, Computer-aided retinal vessel segmentation in retinal images: convolutional neural networks, Multimed. Tools Appl. 80 (2021) 3505–3528.

[172] S. Xu, Z. Chen, W. Cao, F. Zhang, B. Tao, Retinal vessel segmentation algorithm based on residual convolution neural network, Front. Bioeng. Biotechnol. 9 (2021).

[173] M. Chala, B. Nsiri, M.H. El yousfi Alaoui, A. Soulaymani, A. Mokhtari, B. Benaji, An automatic retinal vessel segmentation approach based on convolutional neural networks, Expert Syst. Appl. 184 (2021) 115459.

[174] h. xia, L. Wu, Y. Lan, H. Li, S. Song, HRNet:A hierarchical recurrent convolution neural network for retinal vessel segmentation, Multimedia Tools Appl. (2022).

[175] Y. Xu, Y. Fan, Dual-channel asymmetric convolutional neural network for an efficient retinal blood vessel segmentation in eye fundus images, Biocybern. Biomed. Eng. 42 (2) (2022) 695–706.

[176] S.K. Vengalil, N. Sinha, S.S.S. Kruthiventi, R.V. Babu, Customizing CNNs for blood vessel segmentation from fundus images, in: 2016 International Conference on Signal Processing and Communications, (SPCOM), 2016, pp. 1–4.

[177] D. Mahapatra, P.K. Roy, S. Sedai, R. Garnavi, Retinal image quality classification using saliency maps and CNNs, in: L. Wang, E. Adeli, Q. Wang, Y. Shi, H.-I. Suk (Eds.), Machine Learning in Medical Imaging, Springer International Publishing, Cham, 2016, pp. 172–179.

[178] K. Hu, Z. Zhang, X. Niu, Y. Zhang, C. Cao, F. Xiao, X. Gao, Retinal vessel segmentation of color fundus images using multiscale convolutional neural network with an improved cross-entropy loss function, Neurocomputing 309 (2018) 179–191.

[179] D.E. Alvarado-Carrillo, O.S. Dalmau-Cedeño, Width attention based convolutional neural network for retinal vessel segmentation, Expert Syst. Appl. 209 (2022) 118313.

[180] R.J. Araújo, J.S. Cardoso, H.P. Oliveira, A single-resolution fully convolutional network for retinal vessel segmentation in raw fundus images, in: E. Ricci, S. Rota Bulò, C. Snoek, O. Lanz, S. Messelodi, N. Sebe (Eds.), Image Analysis and Processing – ICIAP 2019, Springer International Publishing, Cham, 2019, pp. 59–69.

[181] J. Long, E. Shelhamer, T. Darrell, Fully convolutional networks for semantic segmentation, CoRR (2014) arXiv:1411.4038.

[182] Y. Luo, H. Cheng, L. Yang, Size-invariant fully convolutional neural network for vessel segmentation of digital retinal images, in: 2016 Asia-Pacific Signal and Information Processing Association Annual Summit and Conference, (APSIPA), 2016, pp. 1–7.

[183] A. Dasgupta, S. Singh, A fully convolutional neural network based structured prediction approach towards the retinal vessel segmentation, in: 2017 IEEE 14th International Symposium on Biomedical Imaging, (ISBI 2017), 2017, pp. 248–251.

[184] Z. Jiang, H. Zhang, Y. Wang, S.-B. Ko, Retinal blood vessel segmentation using fully convolutional network with transfer learning, Comput. Med. Imaging Graph. 68 (2018) 1–15.

[185] A. Oliveira, S. Pereira, C.A. Silva, Retinal vessel segmentation based on fully convolutional neural networks, Expert Syst. Appl. 112 (2018) 229–242.

[186] Y. Jiang, H. Zhang, N. Tan, L. Chen, Automatic retinal blood vessel segmentation based on fully convolutional neural networks, Symmetry 11 (9) (2019).

[187] J. Lyu, P. Cheng, X. Tang, Fundus image based retinal vessel segmentation utilizing a fast and accurate fully convolutional network, in: H. Fu, M.K. Garvin, T. MacGillivray, Y. Xu, Y. Zheng (Eds.), Ophthalmic Medical Image Analysis, Springer International Publishing, Cham, 2019, pp. 112–120.

[188] V. Sathananthavathi, G. Indumathi, A. Swetha Ranjani, Parallel architecture of fully convolved neural network for retinal vessel segmentation, J. Digital Imaging 33 (2020) 168–180.

[189] T.A. Soomro, A.J. Afifi, J. Gao, O. Hellwich, L. Zheng, M. Paul, Strided fully convolutional neural network for boosting the sensitivity of retinal blood vessels segmentation, Expert Syst. Appl. 134 (2019) 36–52.

[190] T.M. Khan, S.S. Naqvi, M. Arsalan, M.A. Khan, H.A. Khan, A. Haider, Exploiting residual edge information in deep fully convolutional neural networks for retinal vessel segmentation, in: 2020 International Joint Conference on Neural Networks, (IJCNN), 2020, pp. 1–8.

[191] T.M. Khan, A. Robles-Kelly, S.S. Naqvi, RC-net: A convolutional neural network for retinal vessel segmentation, in: 2021 Digital Image Computing: Techniques and Applications, (DICTA), 2021, pp. 01–07.

[192] I. Atli, O.S. Gedik, Sine-net: A fully convolutional deep learning architecture for retinal blood vessel segmentation, Eng. Sci. Technol. Int. J. 24 (2) (2021) 271–283.

[193] P.M. Samuel, T. Veeramalai, VSSC net: Vessel specific skip chain convolutional network for blood vessel segmentation, Comput. Methods Programs Biomed. 198 (2021) 105769.

[194] K.-B. Park, S.H. Choi, J.Y. Lee, M-GAN: Retinal blood vessel segmentation by balancing losses through stacked deep fully convolutional networks, IEEE Access 8 (2020) 146308–146322.

[195] O. Ronneberger, P. Fischer, T. Brox, U-net: Convolutional networks for biomedical image segmentation, in: N. Navab, J. Hornegger, W.M. Wells, A.F. Frangi (Eds.), Medical Image Computing and Computer-Assisted Intervention – MICCAI 2015, Springer International Publishing, Cham, 2015, pp. 234–241.

[196] Q. Li, S. Zhong, Z. Chen, X. Zhou, G. Yang, H. Zhang, T. Wang, A high-speed end-to-end approach for retinal arteriovenous segmentation, in: 2017 10th International Congress on Image and Signal Processing, BioMedical Engineering and Informatics, (CISP-BMEI), 2017, pp. 1–5.

[197] X. Gao, Y. Cai, C. Qiu, Y. Cui, Retinal blood vessel segmentation based on the Gaussian matched filter and U-net, in: 2017 10th International Congress on Image and Signal Processing, BioMedical Engineering and Informatics, (CISP-BMEI), IEEE, 2017, pp. 1–5.

[198] D. Wang, A. Haytham, J. Pottenburgh, O. Saeedi, Y. Tao, Hard attention net for automatic retinal vessel segmentation, IEEE J. Biomed. Health Inf. 24 (12) (2020) 3384–3396.

[199] X. Li, Y. Jiang, M. Li, S. Yin, Lightweight attention convolutional neural network for retinal vessel image segmentation, IEEE Trans. Ind. Inform. 17 (3) (2021) 1958–1967.

[200] T. Mostafiz, I. Jarin, S.A. Fattah, C. Shahnaz, Retinal blood vessel segmentation using residual block incorporated U-net architecture and fuzzy inference system, in: 2018 IEEE International WIE Conference on Electrical and Computer Engineering, (WIECON-ECE), IEEE, 2018, pp. 106–109.

[201] T.A. Soomro, A.J. Afifi, J. Gao, O. Hellwich, M. Paul, L. Zheng, Strided U-net model: Retinal vessels segmentation using dice loss, in: 2018 Digital Image Computing: Techniques and Applications, (DICTA), 2018, pp. 1–8.

[202] L. Luo, D. Chen, D. Xue, Retinal blood vessels semantic segmentation method based on modified U-net, in: 2018 Chinese Control and Decision Conference, (CCDC), 2018, pp. 1892–1895.

[203] M.Z. Alom, M. Hasan, C. Yakopcic, T.M. Taha, V.K. Asari, Recurrent residual convolutional neural network based on u-net (r2u-net) for medical image segmentation, 2018, arXiv preprint arXiv:1802.06955.

[204] X. Xu, T. Tan, F. Xu, An improved U-net architecture for simultaneous arteriole and venule segmentation in fundus image, in: M. Nixon, S. Mahmoodi, R. Zwiggelaar (Eds.), Medical Image Understanding and Analysis, Springer International Publishing, Cham, 2018, pp. 333–340.

[205] A. Galdran, P. Costa, A. Bria, T. Araújo, A.M. Mendonça, A. Campilho, A no-reference quality metric for retinal vessel tree segmentation, in: A.F. Frangi, J.A. Schnabel, C. Davatzikos, C. Alberola-López, G. Fichtinger (Eds.), Medical Image Computing and Computer Assisted Intervention – MICCAI 2018, Springer International Publishing, Cham, 2018, pp. 82–90.

[206] Z. Yan, X. Yang, K.-T. Cheng, Joint segment-level and pixel-wise losses for deep learning based retinal vessel segmentation, IEEE Trans. Biomed. Eng. 65 (9) (2018) 1912–1923.

[207] Y. Zhang, A.C.S. Chung, Deep supervision with additional labels for retinal vessel segmentation task, in: A.F. Frangi, J.A. Schnabel, C. Davatzikos, C. Alberola-López, G. Fichtinger (Eds.), Medical Image Computing and Computer Assisted Intervention – MICCAI 2018, Springer International Publishing, Cham, 2018, pp. 83–91.

[208] C. Wang, Z. Zhao, Q. Ren, Y. Xu, Y. Yu, Dense U-net based on patch-based learning for retinal vessel segmentation, Entropy 21 (2) (2019).

[209] Z. Luo, Y. Zhang, L. Zhou, B. Zhang, J. Luo, H. Wu, Micro-vessel image segmentation based on the AD-unet model, IEEE Access 7 (2019) 143402–143411.

[210] T.A. Soomro, A.J. Afifi, A. Ali Shah, S. Soomro, G.A. Baloch, L. Zheng, M. Yin, J. Gao, Impact of image enhancement technique on CNN model for retinal blood vessels segmentation, IEEE Access 7 (2019) 158183–158197.

[211] Q. Jin, Z. Meng, T.D. Pham, Q. Chen, L. Wei, R. Su, DUNet: A deformable network for retinal vessel segmentation, Knowl.-Based Syst. 178 (2019) 149–162.

[212] R. Biswas, A. Vasan, S.S. Roy, Dilated deep neural network for segmentation of retinal blood vessels in fundus images, Iran. J. Sci. Technol., Trans. Electr. Eng. 44 (1) (2020) 505–518.

[213] H. Ding, X. Cui, L. Chen, K. Zhao, MRU-net: A U-shaped network for retinal vessel segmentation, Appl. Sci. 10 (19) (2020).

[214] Y. Cheng, M. Ma, L. Zhang, C. Jin, L. Ma, Y. Zhou, Retinal blood vessel segmentation based on densely connected U-net, Math. Biosci. Eng. 17 (4) (2020) 3088–3108.

[215] L. Mou, L. Chen, J. Cheng, Z. Gu, Y. Zhao, J. Liu, Dense dilated network with probability regularized walk for vessel detection, IEEE Trans. Med. Imaging 39 (5) (2020) 1392–1403.

[216] A. Reyes-Figueroa, M. Rivera, W-net: A convolutional neural network for retinal vessel segmentation, in: E. Roman-Rangel, A.F. Kuri-Morales, J.F. Martínez-Trinidad, J.A. Carrasco-Ochoa, J.A. Olvera-López (Eds.), Pattern Recognition, Springer International Publishing, Cham, 2021, pp. 355–368.

[217] C. Chen, J.H. Chuah, R. Ali, Retinal vessel segmentation in fundus images using convolutional neural network, in: 2021 International Conference on High Performance Big Data and Intelligent Systems, 2021, pp. 261–265.

[218] M. Sun, K. Li, X. Qi, H. Dang, G. Zhang, Contextual information enhanced convolutional neural networks for retinal vessel segmentation in color fundus images, J. Vis. Commun. Image Represent. 77 (2021) 103134.

[219] D.E. Alvarado-Carrillo, E. Ovalle-Magallanes, O.S. Dalmau-Cedeño, D-GaussianNet: Adaptive distorted Gaussian matched filter with convolutional neural network for retinal vessel segmentation, in: M. Nguyen, W.Q. Yan, H. Ho (Eds.), Geometry and Vision, Springer International Publishing, Cham, 2021, pp. 378–392.

[220] L. Yang, H. Wang, Q. Zeng, Y. Liu, G. Bian, A hybrid deep segmentation network for fundus vessels via deep-learning framework, Neurocomputing 448 (2021) 168–178.

[221] K. Li, X. Qi, Y. Luo, Z. Yao, X. Zhou, M. Sun, Accurate retinal vessel segmentation in color fundus images via fully attention-based networks, IEEE J. Biomed. Health Inform. 25 (6) (2021) 2071–2081.

[222] J. Wu, Y. Liu, Y. Zhu, Z. Li, Atrous residual convolutional neural network based on U-net for retinal vessel segmentation, PLOS ONE 17 (8) (2022) 1–16.

[223] Y. Zhang, J. Fang, Y. Chen, L. Jia, Edge-aware U-net with gated convolution for retinal vessel segmentation, Biomed. Signal Process. Control 73 (2022) 103472.

[224] Y. Zhang, M. He, Z. Chen, K. Hu, X. Li, X. Gao, Bridge-net: Context-involved U-net with patch-based loss weight mapping for retinal blood vessel segmentation, Expert Syst. Appl. 195 (2022) 116526.

[225] D. Yang, H. Zhao, T. Han, Learning feature-rich integrated comprehensive context networks for automated fundus retinal vessel analysis, Neurocomputing 491 (2022) 132–143.

[226] F. Dong, D. Wu, C. Guo, S. Zhang, B. Yang, X. Gong, CRAUNet: A cascaded residual attention U-net for retinal vessel segmentation, Comput. Biol. Med. 147 (2022) 105651.

[227] H. Wang, G. Xu, X. Pan, Z. Liu, N. Tang, R. Lan, X. Luo, Attention-inception-based U-net for retinal vessel segmentation with advanced residual, Comput. Electr. Eng. 98 (2022) 107670.

[228] Z. Zhu, Q. An, Z. Wang, Q. Li, H. Fang, Z. Huang, ILU-net: Inception-like U-net for retinal vessel segmentation, Optik 260 (2022) 169012.

[229] X. Yang, Z. Li, Y. Guo, D. Zhou, DCU-net: A deformable convolutional neural network based on cascade U-net for retinal vessel segmentation, Multimedia Tools Appl. 81 (11) (2022) 15593–15607.

[230] S. Hussain, F. Guo, W. Li, Z. Shen, DilUnet: A U-net based architecture for blood vessels segmentation, Comput. Methods Programs Biomed. 218 (2022) 106732.

[231] J. Zhang, W. Wang, Retinal vessel segmentation based on U-net network, in: 2022 2nd International Conference on Consumer Electronics and Computer Engineering, (ICCECE), 2022, pp. 380–383.

[232] D. Herrera, G. Ochoa-Ruiz, M. Gonzalez-Mendoza, C. Mata, Impact of loss function in deep learning methods for accurate retinal vessel segmentation, 2022, http://dx.doi.org/10.48550/ARXIV.2206.00536.

[233] I. Goodfellow, J. Pouget-Abadie, M. Mirza, B. Xu, D. Warde-Farley, S. Ozair, A. Courville, Y. Bengio, Generative adversarial nets, in: Z. Ghahramani, M. Welling, C. Cortes, N. Lawrence, K. Weinberger (Eds.), Advances in Neural Information Processing Systems, Vol. 27, Curran Associates, Inc., 2014.

[234] W. Tu, W. Hu, X. Liu, J. He, DRPAN: A novel adversarial network approach for retinal vessel segmentation, in: 2019 14th IEEE Conference on Industrial Electronics and Applications, (ICIEA), 2019, pp. 228–232.

[235] Z. Gu, J. Cheng, H. Fu, K. Zhou, H. Hao, Y. Zhao, T. Zhang, S. Gao, J. Liu, CE-net: Context encoder network for 2D medical image segmentation, IEEE Trans. Med. Imaging 38 (10) (2019) 2281–2292.

[236] C. Wu, Y. Zou, Z. Yang, U-GAN: Generative adversarial networks with U-net for retinal vessel segmentation, in: 2019 14th International Conference on Computer Science & Education, (ICCSE), 2019, pp. 642–646.

[237] Y. Dong, W. Ren, K. Zhang, Deep supervision adversarial learning network for retinal vessel segmentation, in: 2019 12th International Congress on Image and Signal Processing, BioMedical Engineering and Informatics, (CISP-BMEI), 2019, pp. 1–6.

[238] A. Lahiri, V. Jain, A. Mondal, P.K. Biswas, Retinal vessel segmentation under extreme low annotation: A gan based semi-supervised approach, in: 2020 IEEE International Conference on Image Processing, (ICIP), 2020, pp. 418–422.

[239] T. Yang, T. Wu, L. Li, C. Zhu, SUD-GAN: deep convolution generative adversarial network combined with short connection and dense block for retinal vessel segmentation, J. Digital Imaging 33 (4) (2020) 946–957.

[240] Y. Ma, Y. Hua, H. Deng, T. Song, H. Wang, Z. Xue, H. Cao, R. Ma, H. Guan, Self-supervised vessel segmentation via adversarial learning, in: Proceedings of the IEEE/CVF International Conference on Computer Vision, (ICCV), 2021, pp. 7536–7545.

[241] Y. Zhou, Z. Chen, H. Shen, X. Zheng, R. Zhao, X. Duan, A refined equilibrium generative adversarial network for retinal vessel segmentation, Neurocomputing 437 (2021) 118–130.

[242] J. Zhao, Q. Feng, Deep att-ResGAN: A retinal vessel segmentation network for color fundus images., Trait. Signal 38 (5) (2021).

[243] M. Yang, Y. Ye, K. Ye, X. Hu, B. Hu, Retinal vessel segmentation using multi-scale generative adversarial network with class activation mapping, in: X. Gao, A. Jamalipour, L. Guo (Eds.), Wireless Mobile Communication and Healthcare, Springer International Publishing, Cham, 2022, pp. 95–105.

[244] M.K. Kar, D.R. Neog, M.K. Nath, Retinal vessel segmentation using multi-scale residual convolutional neural network (MSR-net) combined with generative adversarial networks, Circuits Systems Signal Process. (2022) 1–30.

[245] A. Alimanov, M.B. Islam, Retinal image restoration and vessel segmentation using modified cycle-CBAM and CBAM-unet, 2022, http://dx.doi.org/10.48550/ARXIV.2209.04234.

[246] G. Lin, H. Bai, J. Zhao, Z. Yun, Y. Chen, S. Pang, Q. Feng, Improving sensitivity and connectivity of retinal vessel segmentation via error discrimination network, Med. Phys. (2022).

[247] C. Yue, M. Ye, P. Wang, D. Huang, X. Lu, Generative adversarial network combined with SE-ResNet and dilated inception block for segmenting retinal vessels, Comput. Intell. Neurosci. 2022 (2022).

[248] C. Yue, M. Ye, P. Wang, D. Huang, X. Lu, SRV-GAN: A generative adversarial network for segmenting retinal vessels, Math. Biosci. Eng. 19 (10) (2022) 9948–9965.

[249] W. Gu, Y. Xu, Retinal vessel segmentation via adversarial learning and iterative refinement, J. Shanghai Jiaotong Univ. (Sci.) (2022) 1–8.

[250] N. Liang, L. Yuan, X. Wen, H. Xu, J. Wang, End-to-end retina image synthesis based on CGAN using class feature loss and improved retinal detail loss, IEEE Access 10 (2022) 83125–83137.